# VAPOR DEPOSITION EQUIPMENT AND THIN FILM PROCESSING

FINAL PROGRESS REPORT

P.J.Gielisse, H.Niculescu, Y.Xu, N.Bai and M.Tu

August 1996

U.S. Army Research Office
DAAH04-93-G-0492

Florida A&M University/Florida State University
College of Engineering
2525 Pottsdamer Street
Tallahassee, FL 32310



APPROVED FOR PUBLIC RELEASE
DISTRIBUTION UNLIMITED

SF 298 MASTER COPY KEEP THIS COPY FOR REPRODUCTION PURPOSES

# REPORT DOCUMENTATION PAGE

*Form Approved OMB NO. 0704-0188*



| 1. AGENCY USE ONLY *(Leave blank)* | 2. REPORT DATE | 3. REPORT TYPE AND DATES COVERED |
|---|---|---|
| | | |

**4. TITLE AND SUBTITLE**

Vapor Deposition Equipment and Thin Film Processing

**5. FUNDING NUMBERS**

DAAH04-93-G-0492

**6. AUTHOR(S)**

Peter J. Gielisse, Halina Niculescu, Yang Xu, Nai-Zhi Bai and Meirong Tu

**7. PERFORMING ORGANIZATION NAMES(S) AND ADDRESS(ES)**

Florida A&M University/Florida State University,
College of Engineering,
2525 Pottsdamer St.
Tallahassee, FL 32310-6046

**8. PERFORMING ORGANIZATION REPORT NUMBER**

_____

**9. SPONSORING / MONITORING AGENCY NAME(S) AND ADDRESS(ES)**

U.S. Army Research Office
P.O. Box 12211
Research Triangle Park, NC 27709-2211

**10. SPONSORING / MONITORING AGENCY REPORT NUMBER**

ARO 32461.1-MS-ISP

**11. SUPPLEMENTARY NOTES**

The views, opinions and/or findings contained in this report are those of the author(s) and should not be construed as an official Department of the Army position, policy or decision, unless so designated by other documentation.

**12a. DISTRIBUTION / AVAILABILITY STATEMENT**

Approved for public release; distribution unlimited.

**12 b. DISTRIBUTION CODE**

**13. ABSTRACT** *(Maximum 200 words)*

Work under the contract has provided a vapor deposition facility for the generation of thin films and film strctures (devices) for structural and electronic applications.

Efforts have been expanded into the actual deposition of films in the systems AlN, (Al,B)N, c-BN (cubic boron nitride) and Si-Al-O-N.

We report on the resultant physical, chemical, materials and electronic properties and surface characteristics of the films. In certain cases multilayer film structures have been characterized as well.

Device application include high thermal conductivity electronic substrates, device coatings, energy storage capacitor structures, electron emission surfaces (cold cathodes) and low-wear high-strength materials.

| 14. SUBJECT TERMS | 15. NUMBER IF PAGES |
|---|---|
| Physical vapor deposition;Chemical vapor deposition; Thin films Aluminum nitride; Boron nitride; Sialon; Capacitors; Substrates; High bandgap materials; Electronic devices; (to be continued) | 49 |
| | 16. PRICE CODE |

| 17. SECURITY CLASSIFICATION OR REPORT | 18. SECURITY CLASSIFICATION OF THIS PAGE | 19. SECURITY CLASSIFICATION OF ABSTRACT | 20. LIMITATION OF ABSTRACT |
|---|---|---|---|
| UNCLASSIFIED | UNCLASSIFIED | UNCLASSIFIED | UL |

## REPORT DOCUMENTATION PAGE (SF298)
(Continuation Sheet)

14. SUBJECT TERMS (continued)

Energy storage; Thermal conductivity; Electronic substrates.

# Contents

# List of Figures

# List of Tables

## ABSTRACT

Work under the contract has provided a vapor deposition facility for the generation of thin films and film structures (devices) for structural and electronic applications.

Efforts have been expanded into the actual deposition of films in the systems $AlN$, $(Al, B)N$, $c\text{-}BN$ (cubic boron nitride) and $Si$ - $Al$ - $O$ - $N$.

We report on the resultant physical, chemical, materials and electronic properties and surface characteristics of the films. In certain cases multilayer film structures have been characterized as well.

Device applications include high thermal conductivity electronic substrates, device coatings, energy storage capacitor structures, electron emission surfaces (cold cathodes) and low-wear high-strength materials.

# 1 Experimental Equipment and Procedures

## 1.1 Equipment

An Edwards vacuum coating unit (model E306A), was used for the initial coating tasks. A base chamber pressure of about 8 $\times 10^{-6}$ torr could routinely be reached with the rotary pump station coupled to a diffusion pump. A Varian ratiomatic ionization gauge is used as a pressure monitor, along with thermocouple type gauges and a Penning gauge for the intermediate vacuum levels.

An MDX type DC magnetron drive, 110 W, is used for the sputtering from metallic targets. For sputtering from an insulator target, an RF 10 (13.56 MHz) RF generator, 110W is available. The front surface of a cold cathode holds the target material to be deposited. Substrates are placed on the grounded anode. The sputtering chamber is back-filled with inert or reactive (sputtering) gas, at various pressures around 0.1 torr. A plasma is generated in the gaseous environment between the electrodes.

A special electronic controller monitors the flow of gas and thus the chamber pressure. Pressure can be adjusted to high levels of precision which optimizes the system for stability, accuracy and response to transients. A quartz crystal thin film deposition monitor is used to determine film thickness and deposition rate by the well established "crystal microbalance technique". It requires input of the values of the film material's density and its acoustic impedance. An in-house fabricated sample stage heated the various substrates to $300^0$C, while a commercial unit can extend the temperature range to $800^0$C.

The magnetron sputtering system, schematically shown in Fig. 1 and in front view in Fig. 2, had the substrate holder positioned at $80^0$ to the chamber's axis. The magnetron source to substrate distance was approximately 12 cm. The quartz crystal holder was mounted at the same angle as the substrate and at the same distance from the magnetron source. At this distance the substrate surface is completely immersed in the plasma but is well removed from the plasma confinement region of the sputtering source.

## 1.2 Substrates and deposition surfaces

Film substrates require a suitable combination of mechanical, thermal, chemical and electrical properties for optimum performance. They should have sufficient mechanical strength to render appropriate support, while a thermal expansion coefficient, preferably matching that of the desired film and a high thermal conductivity, are also important prerequisites. Good thermal shock resistance is important as well. Electrical properties depend on the desired type of application, although one normally aims at a high resistivity and a reasonably low

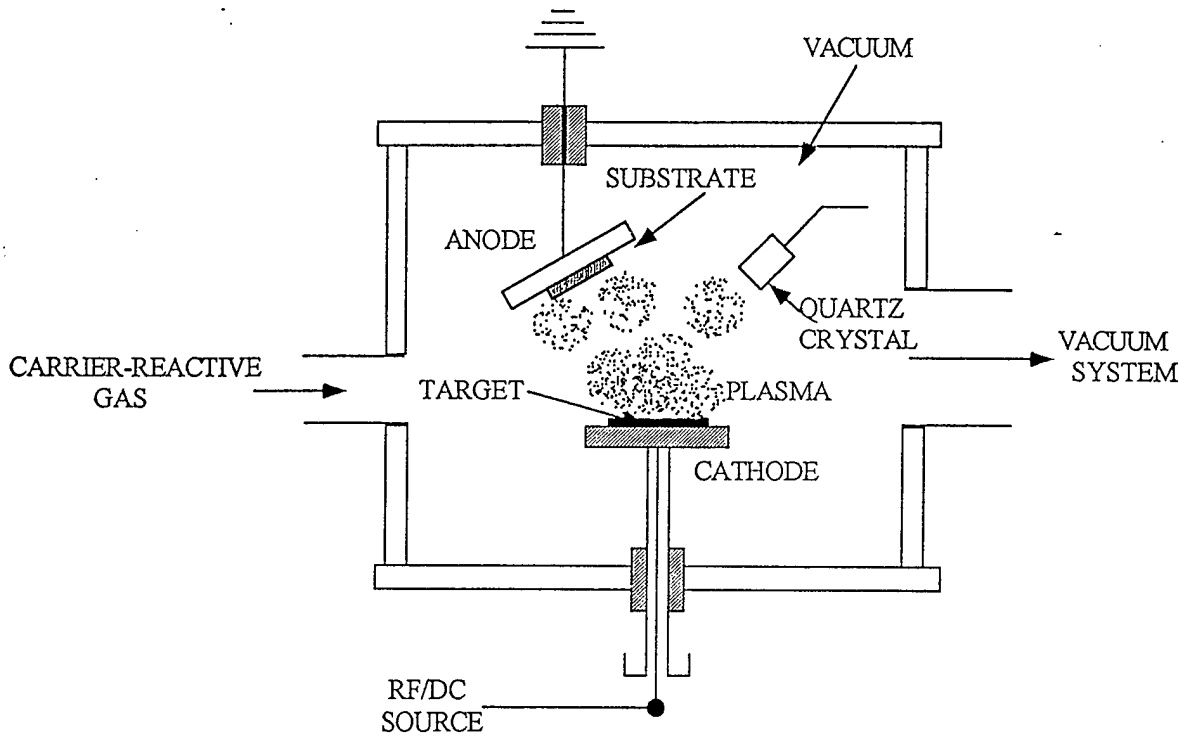


Figure 1: The magnetron sputtering system (schematic).

dielectric constant for multichip module (MCM) applications. The chemistry and structure of the interface should yield excellent adhesion without causing detrimental chemical reactions. Based on the above criteria, we have selected polycrystalline $Al_2O_3$, $MgO$, $AlN$ and single crystal $Si$, (001) and (111), as substrate surfaces in all our thin film depositions.

Surface character of the substrate is also critical particularly in epitaxial thin film deposition. Thinner films are more sensitive to surface irregularities and consequently most of our substrates were lapped and polished to a one (1) microinch RMS finish. This also tended to promote adhesion between film and substrate. We have analyzed surface character with our in-house developed optical scattering technique - digital enhanced scatterometry (DES) - which is capable of operating on -line as a quality control tool [1].

## 1.3 Film deposition rates

We have carried out experiments to determine film deposition rates as a function of reaction gas pressure, the most influential parameter, as well as deposition power and chamber pressure. In general, deposition rates depend on the sputtering power, gas pressure, substrate temperature and the nature of the target material. The results for $AlN$ depositions in nitrogen gas are shown in Fig. 3. Lower gas pressures lead to substantially higher deposition

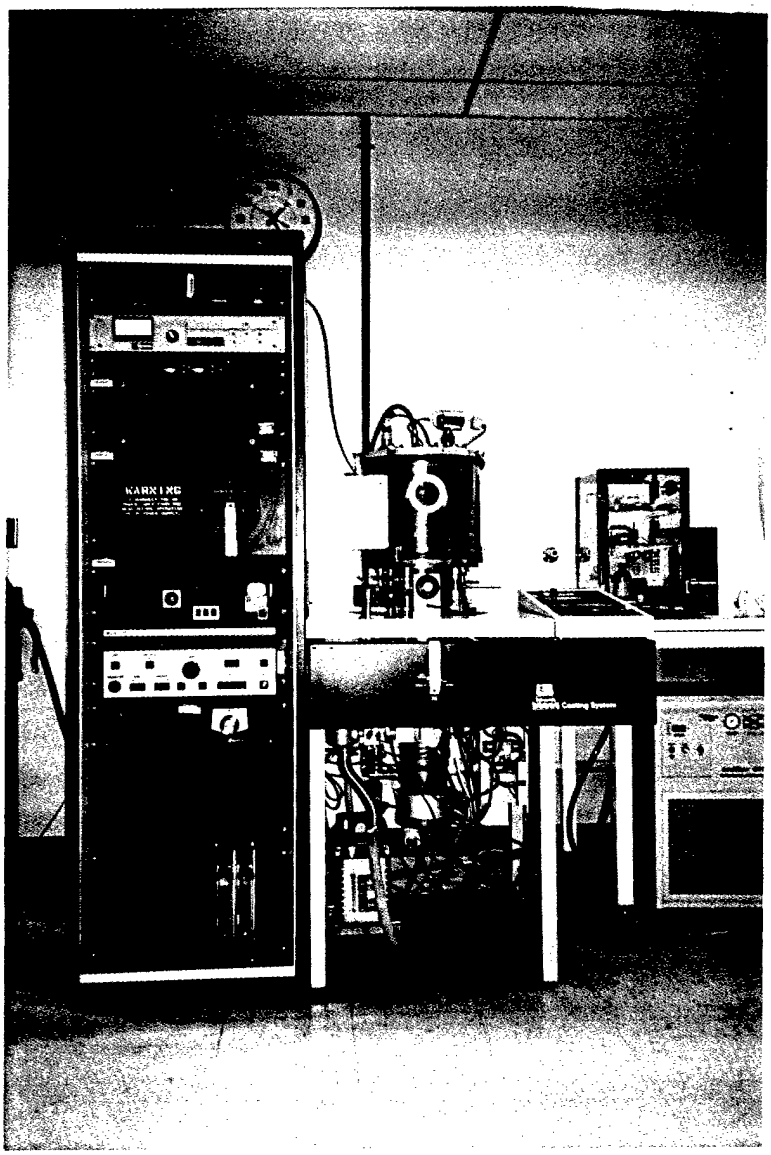

Figure 2: The load-locked sputter deposition system.

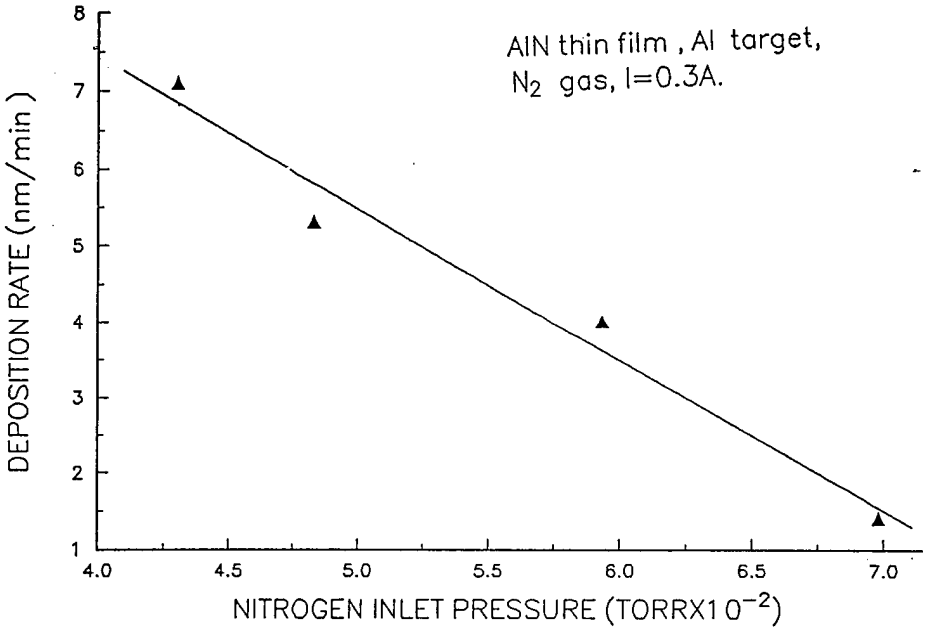


Figure 3: Deposition rate as a function of gas pressure in $AlN$ film deposition.

rates. This effect is likely due to the concomitant higher plasma energies and a lowered sputtered atom-nitrogen gas molecule collision rate. We have not observed critical changes in film quality or surface character at the higher deposition rates.

The sputtering power was found to be proportional to the deposition rate as shown in Fig. 4 for sialon films. At a fixed nitrogen pressure, here 1.7 $\times 10^{-2}$ torr, the rate changes almost linearly from 0 to 4.5 nm/min with a power change from 20 W to 230 W. At a power level below 20 W, the deposition rate showed a negative value indicating that the etching rate was higher than the growth rate.

Another example, Fig. 5, shows the dependence of the growth rate on chamber pressure at 100 W for sialon deposition. The rate increases exponentially with decreasing chamber pressure. The longer mean free path of the particles leads to a decrease in particle collisions in the carrier gas. A plasma could not be maintained at pressures below 3 $\times 10^{-3}$ torr or above 1 $\times 10^{-1}$ torr. The gas ions are too few and have too low an energy at the low pressure end, while a much higher particle density and thus very high collision cross sections, cause the disappearance of the plasma at the higher pressures. The deposition rate studies, Figs. 4-5, were carried out in pure nitrogen to obtain minimum values. Experience indicates that mixed gas environments, e.g. $Ar$ and $N_2$, can readily improve deposition rates by as much as an order of magnitude.

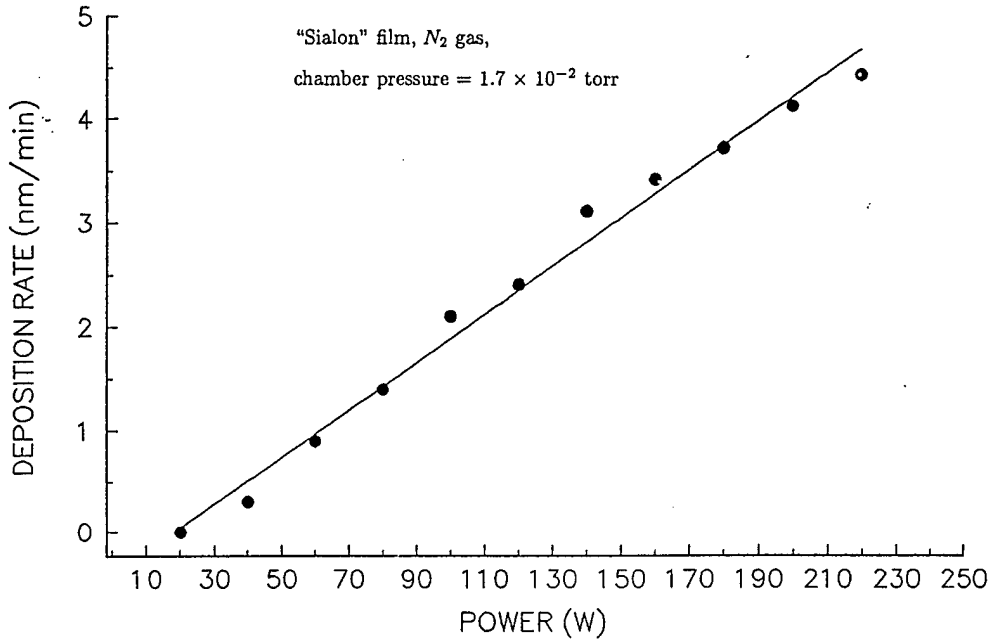


Figure 4: Deposition rate as a function of RF power for sialon type films.

## 1.4 Substrate and film surface character

Whereas the ability to deposit dense (high quality) *AlN* films at high deposition rates (i.e. low cost) is an important objective, equal importance must be attached to the type of surface characteristics of the as-deposited films. Microscopic and SEM investigations of all of our films reveal homogeneous, very smooth, high density continuous surfaces. Examination with our digital enhanced scatterometer (DES) reveals a film surface character that in most cases is enhanced over that of the ultra polished substrates, in RMS roughness, asperity slope and average surface wavelength, see Fig. 6 and Table 1. The ultrasmooth surface character of microelectronic grade silicon, Fig. 7, clearly, constitutes "competition", but only as a result of secondary lapping and polishing operations, i.e extra processing steps. For comparison purposes, Fig. 8 shows the surface character of various substrates.

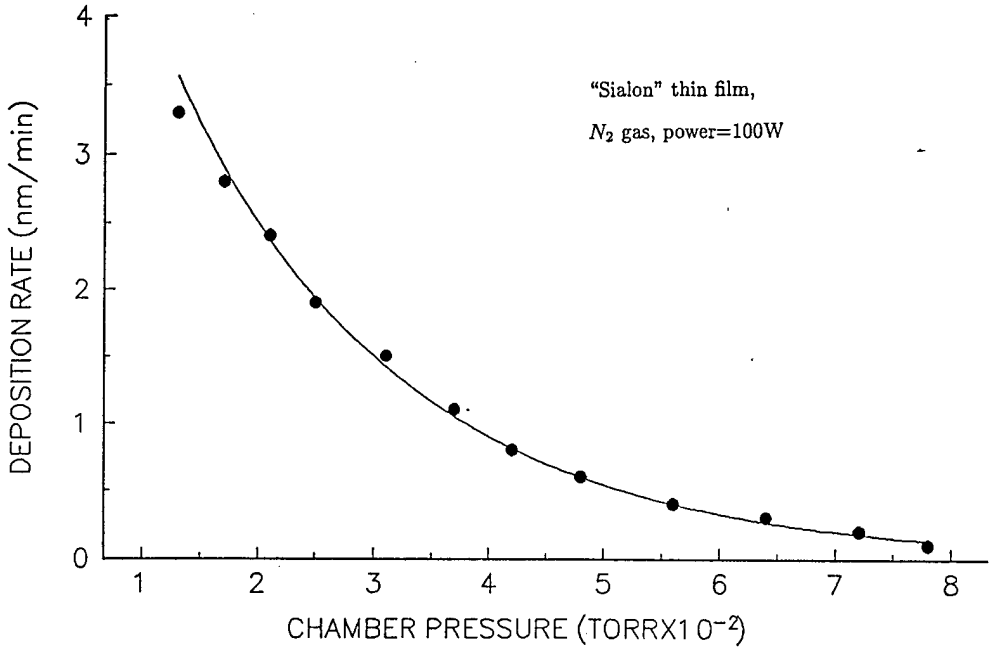


Figure 5: Deposition rate as a function of chamber pressure in sialon film deposition.

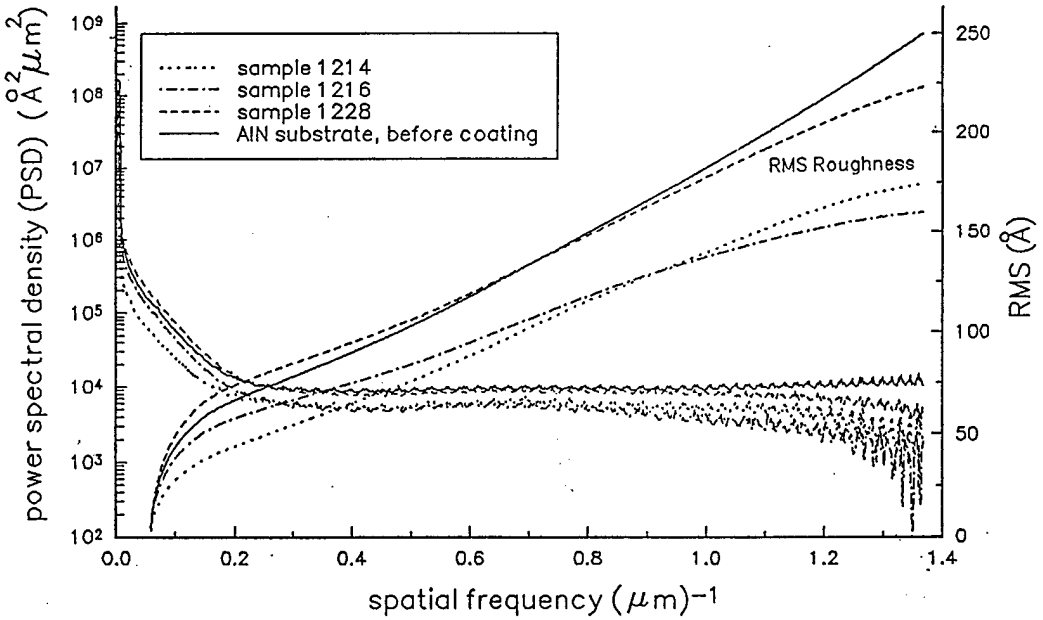


Figure 6: Scatterometry spectra of as-deposited polycrystalline $AlN$ thin films, $\lambda = 632.8nm$.

## TABLE 1

### Surface Data of *AlN* Films and Substrates

| Sample | Roughness, RMS, ( Å) | Asperity slope | Surface wavelength (Å) |
|---|---|---|---|
| *AlN* Film-1214* | 174 | 155 | 7.1 |
| *AlN* Film-1216* | 160 | 129 | 7.8 |
| *AlN* Film-1228* | 223 | 197 | 7.1 |
| *MgO* Substrate | 349 | 350 | 6.3 |
| $Al_2O_3$ Substrate | 300 | 267 | 7.1 |
| *AlN* Substrate (Polished) | 289 | 235 | 7.7 |
| Silicon(001) Substrate (Polished) | 82 | 85 | 6.1 |
| Silicon(111) Substrate (Polished) | 77 | 79 | 6.1 |

* On polished *AlN* substrates

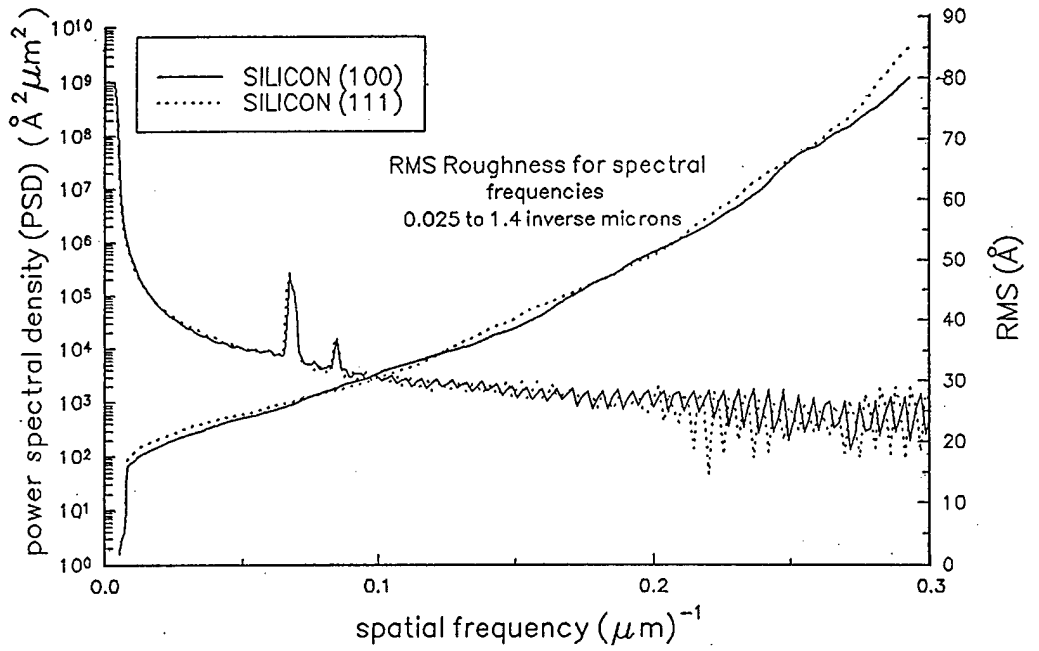


Figure 7: Scatterometry spectra of highly polished electronic grade silicon wafers (substrates), $\lambda = 632.8nm$.

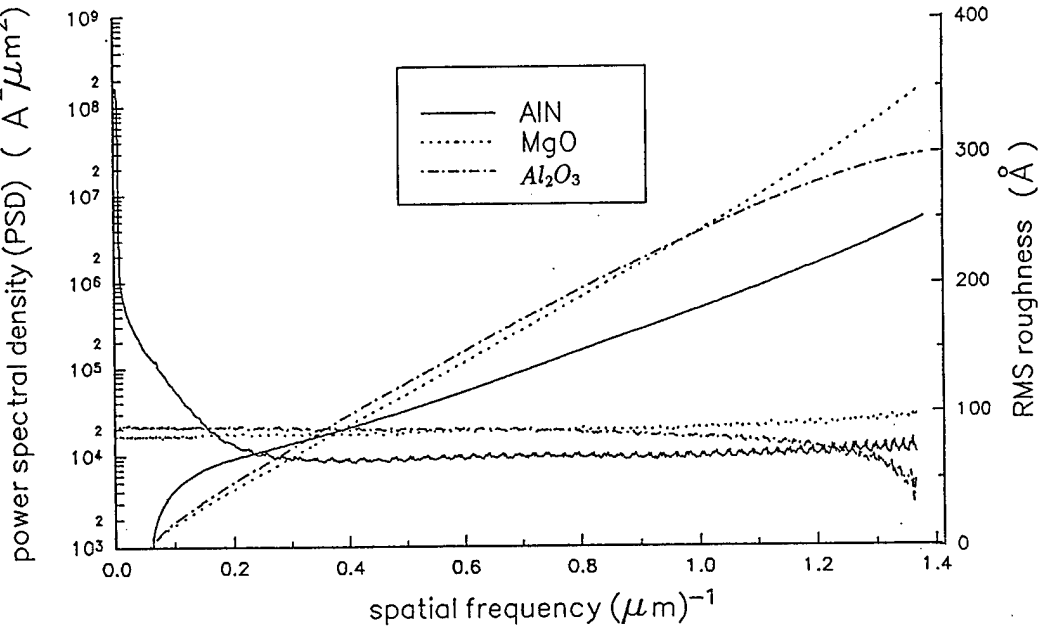


Figure 8: Scatterometry spectra comparing various polycrystalline ceramic substrate materials, $\lambda = 632.8nm$.

# 2 Aluminum Nitride *(AlN)* Thin Film Depositions

## 2.1 General

Aluminum Nitride ($AlN$) crystallizes in the wurtzite structure with lattice constants $a = 3.114\mathring{A}$ and $c = 4.9792\mathring{A}$ [2]. It has a high melting point and high electrical resistivity. It also displays an excellent thermal conductivity (150-230 $Wm^{-1}K^{-1}$), and high chemical and nuclear stability. $AlN$ has therefore a potential for use in optical devices, in surface wave devices, as a material for electrically insulating and passivating layers for semiconductors and in thermal management, from microelectronics to large system substrates.

A combination of attractive physical properties, therefore, makes aluminum nitride ($AlN$) a very promising material for device development. As a wide direct band gap dielectric $AlN$ is thermally and chemically stable, and has a high electrical resistivity. In thin film form it has proven very attractive in the generation and detection of surface and bulk acoustic waves [3-5]. We have ourselves pursued the possibility of using $AlN$ as a device encapsulant in an attempt to reduce the high cost of packaging.

Aluminum nitride films have been prepared by a variety of techniques[6,7] such as sputtering, molecular beam epitaxy (MBE) regular and plasma enhanced chemical vapor deposition (CVD), pyrolitic processes and plasma chemical reactions. The most popular reagents have been $AlCl_3$ and $NH_3$ with substrate temperatures at 700 - 1300$^0$C in RF and microwave energized reactors. The coatings are generally hard and rough with crystallinity, growth behavior and surface morphology, strongly dependent on growth conditions. Growth rates of 1 $\mu$m/min have been reported. Translucent $AlN$ [8] has been obtained by a sintering process, but high thermal conductivity, $>$ 150 $Wm^{-1}K^{-1}$, could only be obtained in materials processed with sintering aids such as $Ca(NO_3)_2$ or $3CaO \cdot Al_2O_3$. The higher thermal conductivity materials have a low $O_2$ content (0.06wt%) as compared to the lower conductivity materials (150$Wm^{-1}K^{-1}$) with an $O_2$ content of 0.2%. CVD has until recently been the most widely employed deposition method. It is said to permit $AlN$ deposition at low substrate temperatures and at high deposition rates [9-11]. It is also felt to be easy to control and high purity $AlN$ can be obtained by this method [12].

We can report the CVD growth of $AlN$ films on $Si$ substrates at moderate temperatures (700 $-$ 800$^0$C) in the pressure range 100 - 650 torr using $AlCl_3$ and $NH_3$ as the source materials.* The layers obtained were highly oriented and uniform. A schematic diagram of the main features of the CVD apparatus used in these experiments is shown in Fig. 9.

*Cooperative work with the University of Missouri, Columbia, Nuclear Engineering Department, 1995-1996.

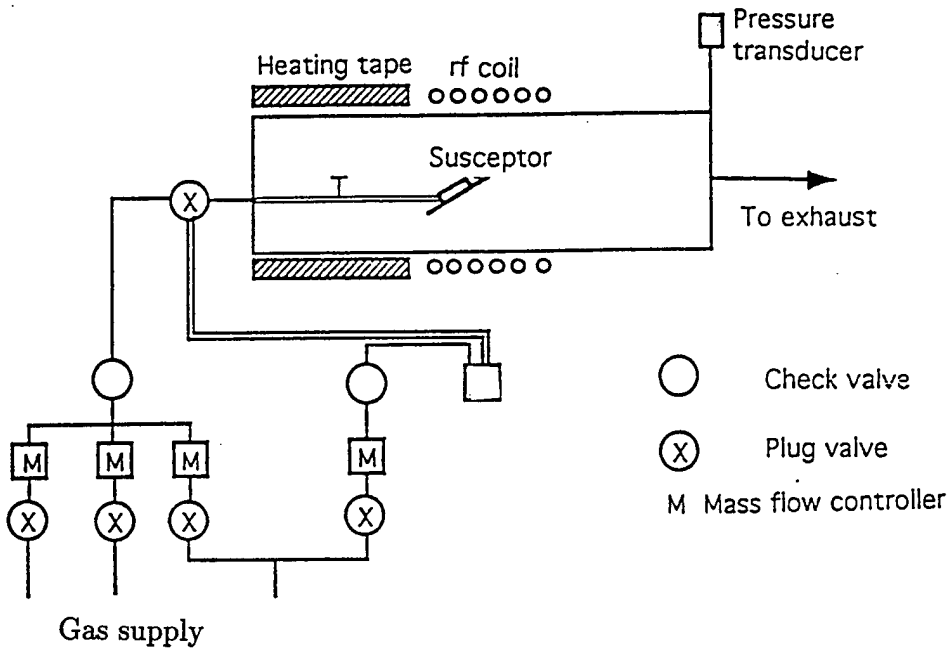


Figure 9: CVD equipment (schematic)

The aluminum chloride is maintained at 150$^0$C to provide sufficient vapor pressure. The gas is carried into the reaction tube by hydrogen at a flow rate of 120 sccm. The flow rate of ammonia is typically 80 sccm with 280 sccm for hydrogen. A part of the reaction tube was maintained at 350$^0$C , using resistance heating, to avoid condensation of ammonium chloride and aluminum chloride-complexes. The overall reaction consists of a range of aluminum chloride-ammonia complexes, and the ammonolysis conversion of the complex into $AlN$ and $HCl$. Prior to growth, the p-type $Si$ (100) substrate with 1-3 ohm-cm resistivity, was cleaned with trichloroethylene, acetone, methanol and de-ionized water in an ultrasonic bath and then briefly annealed in flowing $H_2$ near 500$^0$C prior to growth. About 40 samples at three different experimental conditions were prepared: type 1 samples of $\approx 0.6\mu$m thickness were grown in 15 minutes with the reactor chamber pressure at 650 torr and a substrate temperature of 700$^0$C: Type 2 samples of $\approx 0.9\mu$m thickness were grown in 45 minutes with a chamber pressure of 200 torr and a substrate temperature of 700$^0$C and type 3 samples of $\approx 1\mu$m thickness were grown in 20 minutes with a chamber pressure of 100 torr and substrate temperature of 800$^0$C. Both type 1 and type 3 samples were cooled down in 30 minutes, whereas type 2 samples were cooled down in 5 minutes. All samples appeared to be smooth and showed good interference fringes on these thin ( $\approx 1\mu$m) films.

Although several methods have been used in $AlN$ thin film preparation, such as chemical vapor deposition (CVD)[13-15], reactive molecular beam epitaxy (MBE) [16] and reactive sputtering [17-20], the various DC and RF diode sputtering methods, have been more

commonly used [21-23] of late and appear to be gaining favor in electronic manufacturing applications. Recently Lee et al. [24] reported RF - magnetron - sputtering of $AlN$ thin films onto glass substrates in argon / nitrogen gas mixtures containing 25-75% nitrogen at temperatures below $150^0C$. The c-axis orientation of their $AlN$ films changed from a parallel to a normal to the substrate orientation with a decrease in the sputtering pressure and an increase in the nitrogen concentration. Cross-sections of the $AlN$ films (SEM) clearly showed a columnar growth structure. The grain size at the film surface increased with an increase in the sputtering pressure and a decrease in the nitrogen concentration. The exact surface morphology is important in certain applications such as in piezoelectric substrate applications in which rough surfaces show a large transmission loss.

Penza et al. have also reported on the deposition of $AlN$ films by RF reactive planar magnetron sputtering [25]. Their oriented polycrystalline $AlN$ films were deposited at rates in the range (0.2 - 0.56) $\mu$m/h with an $N_2/Ar$ gas flow ratio of 1:1. They reported structural, compositional and morphological characterization using X-ray diffraction (XRD), X-ray photoelectron spectroscopy (XPS), scanning electron microscopy (SEM) and atomic force microscopy (AFM).

Morito Akiyama et al., [26] reported on the influence of substrate temperature on physical structure of $AlN$ thin films, deposited on polycrystalline $MoSi_2$ by RF magnetron sputtering. The orientation and crystallinity of the polycrystalline hexagonal $AlN$ thin films synthesized at $300^0$C were considered the best of those prepared in the temperature range $(50-500)^0$C.

A variety of substrates, including sapphire [9,27], $\alpha - SiC$ [11,28], quartz [29] and others have been used for the growth of $AlN$ films. Single crystal $a - SiC$ is an ideal substrate for the epitaxial growth of $AlN$ films, having the same structure, nearly the same lattice constant (basal plane), and the same coefficient of thermal expansion (CTE) [30]. Silicon also has nearly the same CTE as $AlN$ and has been used for $AlN$ film growth [11,28]. Epitaxial $AlN$ has been grown by the CVD method [28] on limited areas of $Si$, having an orientation relationship of $AlN$ (0001) onto $Si$ (111) in the temperature range $1100 - 1300^0$C using $AlCl_3$ and $NH_3$.

We have initiated research on the thin film deposition of $AlN$ onto substrates different from those most commonly used so far, specifically, $MgO$, $Al_2O_3$ and $AlN$, in addition to $Si$ (100). The initial results on the sputter deposition of $BN$ films, using low electrical conductivity hexagonal boron nitride ($h - BN$) and boron targets are also presented and discussed here.

Boron nitride ($BN$) thin films have attracted a great deal of interest in recent years not only for their enhanced mechanical, electronic and optical properties but also for the possibility of obtaining $(Al, B)N$ solid solution films. Several research groups have prepared

cubic boron nitride ($c-BN$) films using different methods, e.g. plasma CVD [31], electron cyclotron resonance plasma processes [32] and various PVD techniques like ion plating [33], ion beam assisted deposition [34] and sputtering [35,36], (see further chapter 3, "Deposition of Boron Nitride ($BN$) Films").

Whereas a considerable amount of work has been expended on $AlN$ film and device development, some very important challenges remain. Large area, high quality single crystal films, have not yet been consistently obtained. Cracking, due to differences in the coefficients of expansion between $AlN$ and the substrates, may demand the development of intermediate or graduated layers such as are likely to result from our research in the $Al-B-N$ system. Doping of both $n$ and $p$–type has been accomplished, but not consistently and results from group to group show problems with repeatability. Furthermore, reliable data on majority carrier mobilities are not yet available. Ohmic contacts also need further development. It appears likely, however, that electronic applications, including opto-electronic applications ($AlN$ has a direct band gap) will be accomplished in the near future.

Polycrystalline and amorphous $AlN$ thin films have been fabricated by us on $MgO$, $Al_2O_3$, $Si$ and $AlN$ substrates to average thicknesses from 0.5 to 7 $\mu$m, primarily by DC reactive sputtering from an $Al$ target in $N_2$ atmospheres. All substrates were polycrystalline, except for the (111) and (001) silicon single crystal substrates. A positive voltage was applied to the target, while the substrates were attached to an electrically grounded anode. Input power was varied between 300 and 500W. The nitrogen flow was adjusted relative to pressure changes between 0.001 and 0.005 torr. When the substrates were not intentionally heated, their temperature reached 85$^0$C on the average and the films were amorphous. Crystalline films could be generated with heated substrate temperatures as low as 250$^0$C.

The microstructures of the as-deposited $AlN$ and $BN$ films were examined by scanning electron microscopy (SEM). Crystallinity of these films was verified by X-ray diffractometry.

## 2.2 Experimental results - $AlN$ films

### 2.2.1 Amorphous films

Fig. 10 shows what is typical for our low temperature reactively sputtered $AlN$ depositions on $Al_2O_3$. A very dense, approximately 7 $\mu$m thick film appears to be tightly adhering to the substrate. $AlN$ films on highly polished $AlN$ substrates have much finer surface structures, Fig. 11, while just the opposite is the case with coarse $MgO$ substrates. The film surface appears to "copy" or "mimmick" the substrate character, see e.g., Figs. 10 and 11. Whereas, in the very earliest attempts, the films displayed a variety of colors from blackish brown (high $Al$ concentration) to transparent (stoichiometric), most of our present films are transparent.


Figure 10: $AlN$ film on a ground $Al_2O_3$ substrate.

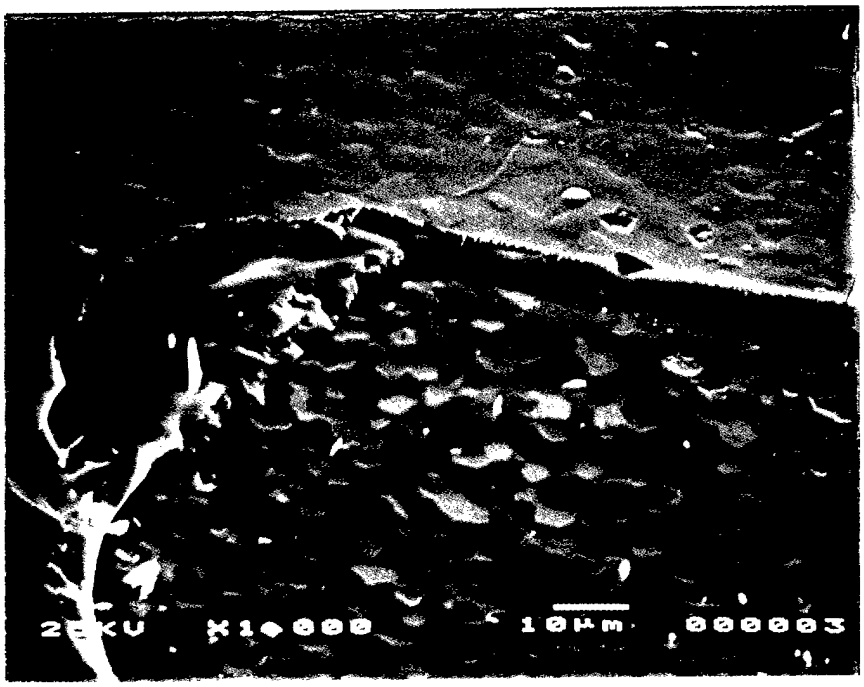


Figure 11: $AlN$ film on a polished $AlN$ substrate.

This is manifested by the visibility of the underlying substrate structure and the formation of interference bands at the films' edges due to retardation effects. In some cases up to seven spectral orders could be observed, forming a sensitive way to gauge minimum thickness of the as-deposited films.

The thicker transparent films also displayed a variety of "bulk" colors, probably due to excess $N$ atoms from the implanted $N^+$ and $N^{+2}$ ions which in turn induce defects creating localized states in the band gap of $AlN$ [37]. The microstructure of the films deposited on relatively coarse substrates is columnar. On the other hand, $AlN$ films deposited on highly polished $AlN$ substrates, (Fig.11) or on the $Si$ substrates, display a highly dense structure without any sign of a "columnar morphology", at least up to a 30,000 magnification.

Treatment after film deposition was found to be very critical. Normal procedure involves leaving the coated substrate in the vacuum environment overnight, allowing for very slow cooling and strain adjustment. If, however, the substrate is removed from the chamber immediately after deposition, residual strain and thermal shock leads to catastrophic destruction and break up of the surface, see e.g., Fig. 12. Note the highly deformed state of these very thin ($\mu$m or less) ceramic films. When not subjected to such a severe shock, we have only occasionally observed much less severe localized cracking or spalling.

The film deposition rate in 100% $N_2$, could be increased by decreasing the gas pressure (constant discharge current of 0.3A). Deposition rates of 0.3$\mu$m/h were obtained at 0.048 torr and 0.08 $\mu$m/h at 0.0698 torr. Order of magnitude improvements are possible with gas mixtures, e.g., 50% argon and 50% nitrogen.

### 2.2.2 Crystalline films

Transparent polycrystalline $AlN$ thin films have been successfully deposited on variously heated substrates. Crystallinity could be maintained at substrate temperatures as low as 250$^0$C. A partial X-ray diffraction pattern for an $AlN$ film on silicon generated at 250$^0$C is shown in Fig. 13. The $2\theta$=33$^0$ peak can be indexed to hexagonal $AlN$ (002). Akiyama et al.[38] produced X-ray diffraction rocking curves of the (002) $AlN$ peak at various substrate temperatures between 200$^0$C ($2\theta \simeq 30^0$) and 300$^0$C ($2\theta \simeq 38^0$). It will be noted that the main diffraction peak of our deposits, at 250$^0$C, falls at an intermediate $2\theta$ value. It can therefore be stated that crystalline films of $AlN$ can be obtained at substrate temperatures as low as 250$^0$ and that the main X-ray peak positions depend on substrate temperature. The higher the temperature, the higher the $2\theta$ value for the (002) peak.

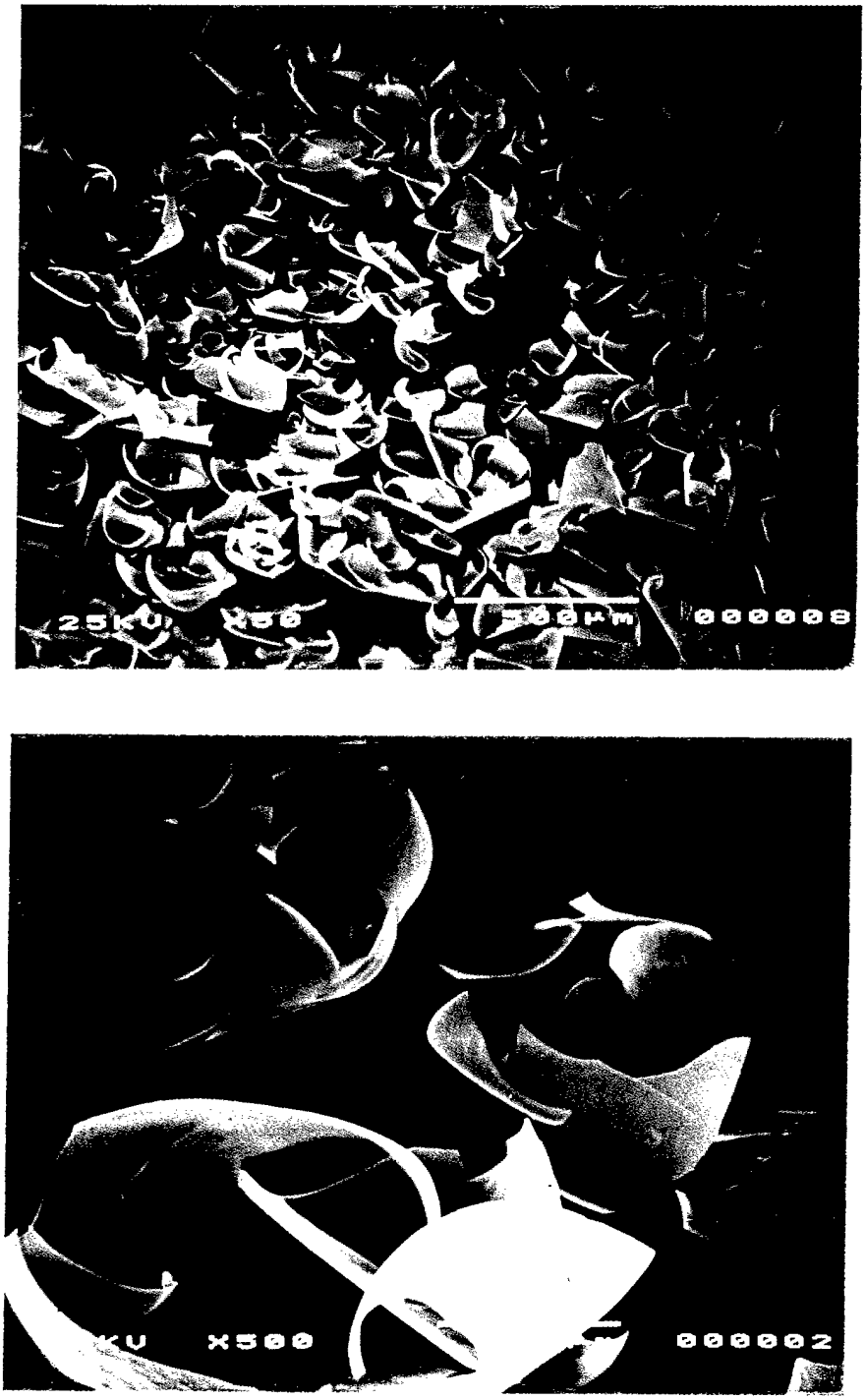


Figure 12: Catastrophic destruction of an $AlN$ thin film surface due to stress release.

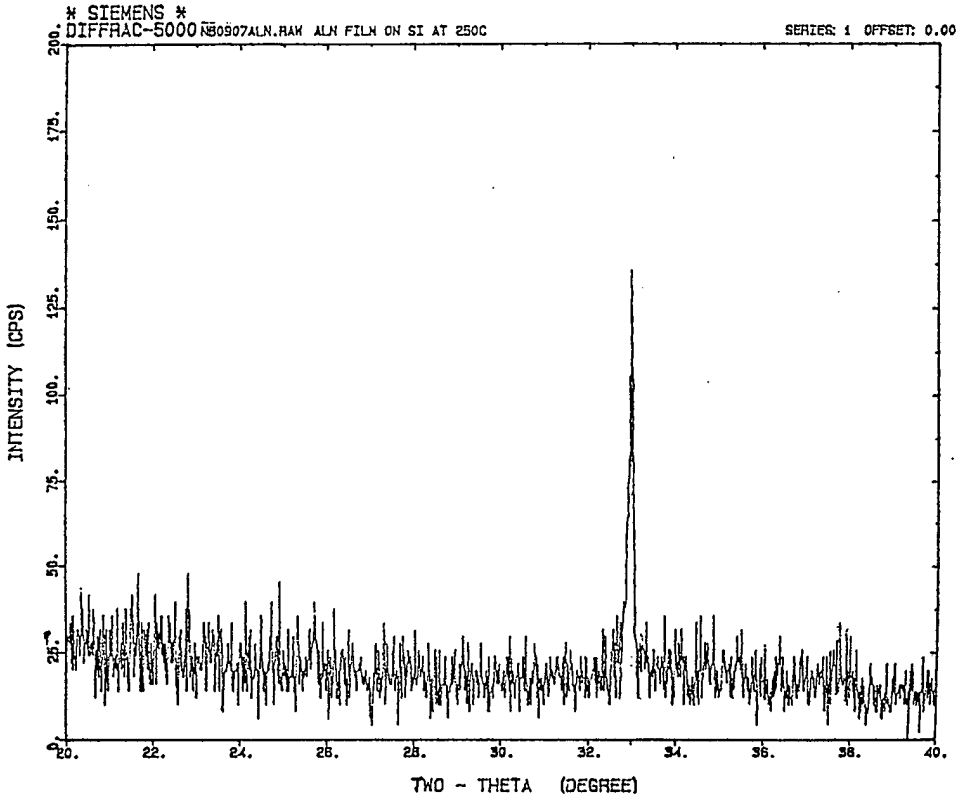


Figure 13: Partial diffraction pattern of an $AlN$ film deposited on a silicon substrate.

# 3 Deposition of Boron Nitride ($BN$) Films

## 3.1 General

The first attempts at low pressure nonequilibrium deposition of $BN$ films were apparently carried out by Sokolowski [39] from a reactive pulse plasma crystallization technique, in which a discharge between $B$ and $Cu$ electrodes in an $N_2 - H_2$ atmosphere resulted in $h - BN$ as the primary phase. Weissmantel et al. [40], used $N_2$ ion beams impinging on evaporated $B$ - targets along with a borazine ($B_3N_3H_6$) precursor. Their results are described as amorphous films with 5 - 20 micrometers $c-BN$ crystallites. The term "$i-BN$" was used. Shanfield and Wolfson [41] accelerated (100 eV) borazine plasma ions onto substrates. X-ray diffraction showed $c - BN$ peaks. Evaporation of boric acid ($H_3BO_3$) in a $NH_3$ plasma by Chopra et al. [42] led to the detection of the product as zincblende $c - BN$ polycrystalline films. The presence of argon in the N-plasma, Inagawa et al. [43], as well as RF heating (up to 600V) of the substrates, promoted the formation of virtually 100% $c - BN$ films. The $BN$ films, about 1000 Å thick, were formed at a deposition rate of 0.05 $\mu$m/min. The microhardness of the 100% $c - BN$ film was estimated as 4000 kg/$mm^2$, a value anticipated for $c - BN$. Wiggins et al. [44] have produced their (1 $\mu$m) $BN$ films through $RF$ diode sputtering. Nitrogen gas contents less than 25% led to deposits high in $B$. Films grown in pure $Ar$ were non-stoichiometric ($B/N > 5.1$) while higher $N_2$ contents led to near stoichiometric $BN$. Film color changed from deep brown (0%$N_2$ - 100% $Ar$) via pale yellow and subsequently to colorless, at higher (> 25%) $N_2$ content. The bandgap value of the films ranged from 3.3 eV (100% $Ar$) to an average of 5.5 eV (100% $N_2$). The bandgap variation could be correlated with excess $B$ content. Arya and D'Amico [45] wrote a review paper in 1988 on the preparation and application of $BN$ films involving chemical deposition (CVD, LPCVD and PECVD), sputtering and various activated (reactive, electron beam) evaporation and ion beam deposition techniques. Deposition temperatures, for various reactant systems, ranged from 250 to 1250°C. The structure of the films was mainly amorphous or polycrystalline (hexagonal or cubic) variable with specific process parameters and with densities falling between 1.7 and 2.1 g/$cm^3$. It was possible to grow stoichiometric $BN$. Ion beam deposition leads to oxygen impurities while the pulsed plasma methods show microinclusions of $B_2O_3$ and boron. Presence of $B$ and $O_2$ leads to moisture sensitivity ($B_2O_3 + 3H_2O \rightarrow 2H_3BO_3$). Otherwise, the $BN$ films are chemically stable (except hot phosphoric acid), are hard (4400 kg/$mm^2$) and adhere satisfactorily to most of the investigated substrates (glass, $Al_2O_3$, $SiO_2$ etc.). Their closing remark, to the effect that low cost $BN$ coatings need improvements in the overall deposition techniques, holds at the time of this writing as much as it did then

(1988). McKenzie and co-workers [46] reported on cubic boron nitride thin films prepared at the Nippon Institute of Technology by a reactive ion plating technique. Boron is evaporated in argon and nitrogen gas with ionization assisted by a tungsten filament, while a magnetic field is applied to a volume ahead of the $Si$ substrate which itself was radio frequency biased and held at a temperature of 250°C. The $BN$ films, in strong biaxial compressive stress (4 GPa), apparently altered their structure to a higher degree of crystallinity in time, with the formation of 20 nm diameter crystallites which could be indexed as $c-BN$. The authors point to the difficulty of interpreting the structure of $BN$ films from diffraction patterns only, because of the almost perfect coincidence of certain principal diffraction features of $c-BN$ and $h-BN$. In analogy to a recent proposal [47] that compressive strain is a factor in promoting $sp^3$ bonding in amorphous carbon films and that this stress component may place the growth conditions above the Berman - Simon line (diamond P - T equilibrium boundary) i.e. in the area where diamond is stable, one might anticipate that similar conditions in $BN$ films should also promote formation of $sp^3$ bonding. Bath et al. [48] have developed a low temperature plasma enhanced chemical vapor deposition technique for the deposition of boron nitride and $InP$ from a borate-dimethylamine [BDMA, $BH_3NH(CH_3)_2$] source containing both boron and nitrogen. The dielectric layers were essentially amorphous or polycrystalline $h-BN$ films with oxygen and carbon contamination, the latter originating from the organometallic precursor. The resistivity of the layers was nevertheless better than 1013 $\Omega \cdot cm$. Komatsu and coworkers [49], in a paper published in December of 1991 remarked that"...there has been no report on the growth of $c-BN$ from the vapor phase where crystallinity is comparable to the CVD diamond." They tried to satisfy the conditions of thermochemical stability and the kinetics of the surface process, as the two prerequisites for nucleation and subsequent growth for CVD growth of $c-BN$, by employing a $BCl_3 + NH_3 + Ar$ plasma in an conductively coupled plasma. The silicon substrate surface, at temperatures of 500 - 900°C, was additionally irradiated by a U.V. laser (193 nm ). Although they did not obtain single phase polycrystalline films, the $c-BN$ and $h-BN$ parts ranked highest in crystallinity as revealed by transmission electron diffraction. The simultaneous use of activated plasma and surface process activation along with the presence of atomic chlorine, yielded the favorable results. In a slightly earlier companion article Komatsu et al. [50] refer to the formation of individual micron size particles deposited in a circular fashion around the periphery of their substrates. The particles did not form without laser excitation of the substrates. From evidence of Auger electron spectroscopy, which indicated a $BN$ composition and the morphological appearance of the particles, the product was considered to be $c-BN$. Doll and coworkers [51] have applied a "physical vapor deposition" method, namely laser ablation of a $BN$ target in $N_2$ atmospheres and have succeeded in generating

several hundred nanometer thick $c-BN$ thin films, heteroepitaxially onto $Si$ (100) targets. The films produced by the pulsed-excimer-laser ablation technique showed no evidence of faceted or granular morphology. The only disturbance of the surface character resulted from micron and submicron features which are thought to be molten boron or $h-BN$ fragments from the target. The lattice constant value of 3.615 Å is in excellent agreement with that for bulk $c-BN$. Sokolowska and Olszyna [52] investigated the influence of electrons, field emitted from a tungsten tip to potentials up to 12 kV, on the crystallization of $c-BN$. Up to a 3 kV potential only $h-BN$ formed. At higher potentials $E-BN$, discovered by Batsanov et al. [53] and considered an intermediate phase between $w-BN$ (wurzite structure) and $c-BN$, resulted. The high temperature - high pressure (HPHT) synthesis of $c-BN$ from $h-BN$ and flux precursor ("catalyst") mixtures, has been well known and highly refined since the original discovery of this diamond structure analog of $BN$ by Wentorf[54] in 1957. A recent review by Vel and coworkers [55], covers this topic very well and is therefore not elaborated on here. HPHT $c-BN$ is so far the only form from which actual device structures have been generated. The first patented passive devices were developed by Gielisse and Dozer [56]. More recently Mishima et al. [57] have grown beryllium doped crystals over $Si$-doped $c-BN$ in solvent - assisted systems at 55 kbar and 2075 K. A p-n junction diode was achieved [58] from the growth product and proved functional up to 650°C. With the ability to grow smooth epitaxial films of $c-BN$ and the proven ability to generate both types of activity in $c-BN$ via doping during growth or implantation techniques, the generation of active, discrete or integrated devices should be realized in the near future. Similar developments in the diamond system - no n-type doping process is known as yet - are not anticipated to be forthcoming at the same rate. HPHT synthesis while possible in principle, cannot be the system of choice for low cost mass - produced devices, certainly not in integrated structures. Further work on $BN$ films finds its justification in the rationale presented above and in the many applications awaiting implementation.

## 3.2 Experimental details

Deposition of $BN$ films was conducted using solid $h-BN$ targets in argon, nitrogen and mixed argon-nitrogen environments. Whereas the deposition pressures and voltages changed somewhat with the choice of the specific gas composition, most runs were made at around $1.7 \times 10^{-2}$ torr and 200 W. The films were deposited on polished silicon (001) and on $AlN$, $Al_2O_3$ and $Ni$, all with and without (low temperature) substrate heating.

The magnetron source - to - substrate distance was kept at approximately 3 cm. At this distance the substrate surface is completely immersed in the plasma. During growth the

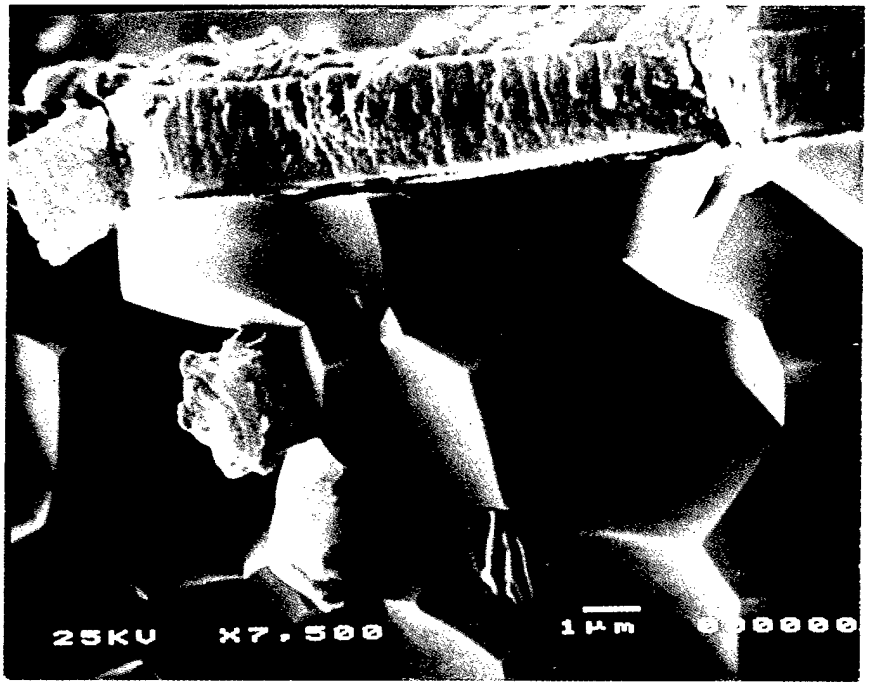


Figure 14: Interface of an as-deposited $BN$ thin film on a superpolished $AlN$ surface, SEM photograph.

chamber pressure was $8.0 \times 10^{-3}$torr using a high purity 50% $Ar$ and 50% $N_2$ atmosphere. Hexagonal boron nitride ($h-BN$) or boron ($B$) targets were used. Due to the low electrical conductivities of $h-BN$ and $B$, sputter deposition of $BN$ films required radio frequency (RF) power at the target electrodes, with the power fixed at 105 W. The reflected power tended to be about 5W and our growth rate was approximately 4 nm per hour.

Figs. 14 and 15 show SEM micrographs of amorphous $BN$ thin films on superpolished $AlN$ and on finely ground $AlN$ substrates. The thin film-substrate interfacial structures appear very different.

## 3.3 Experimental results

### 3.3.1 $BN$ targets - $Si$ substrates

The first films resulting from the low temperature PVD deposition from $h-BN$ targets onto silicon substrates, yielded thick (about 3 $\mu$m), transparent, clean and smooth films. Some cracking and fracturing was observed from time to time in the center portion of the deposits. It is known that boron nitride, in both massive and thin film form, is slowly attacked by water vapor [59]. Thus there were grounds for concern about $BN$ film stability with prolonged exposure to the atmosphere.

Whereas initial microscopic evaluation indicated very smooth essentially featureless films,

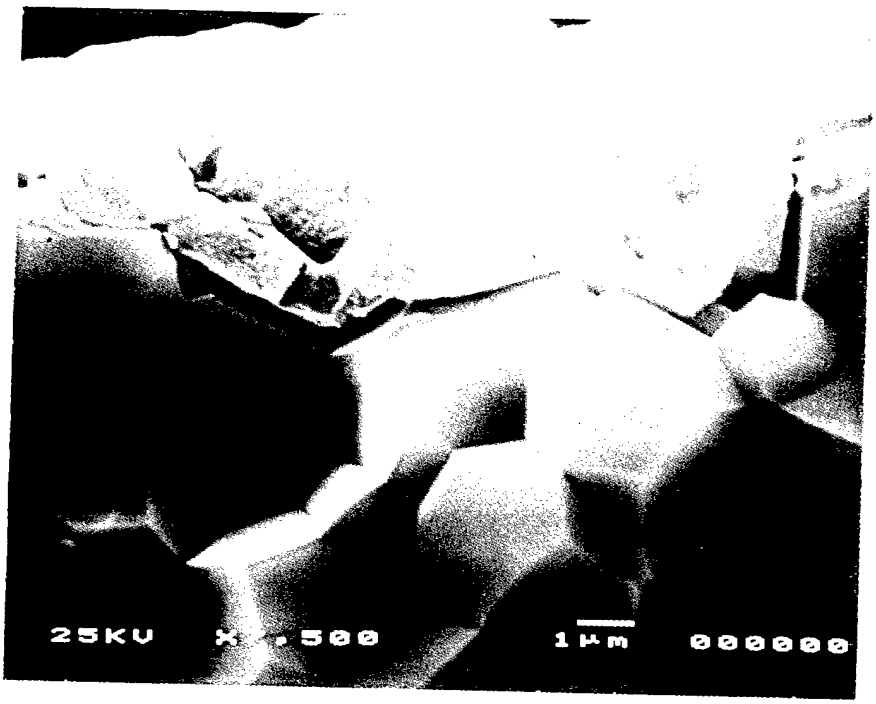


Figure 15: SEM photograph of the interface of an as-deposited $BN$ thin film on ground $AlN$ surface.

reexamination showed distinct surface perturbations over the entire film area. In time, with exposure to laboratory air, it became clear that crystallites had been nucleated and were in effect growing out of the surface at a high rate. This reaction product was transparent, very delicate and thin in cross-section giving the appearance of "butterfly wings", see Fig. 16. X-ray diffraction identified the reaction product as $H_3BO_3$.

Similar depositions with substrate heating between $275^0$ and $300^0$C, yielded only amorphous films. The formation of the "butterfly wings" was noticed in only one case and then only to a minor extent, at these higher substrate temperatures.

We believe that PVD using $h-BN$ targets and low temperature silicon substrates, results in amorphous $h-BN$ films which are rich in free boron and thus highly reactive in moist air environments. With heated substrates, the film is primarily stoichiometric or in any case (more) stable to atmospheric corrosion. Substrate temperatures above $300^0$C are necessary to fully stabilize the surface.

### 3.3.2 $BN$ targets - $AlN$ substrates

In contrast to similar depositions on $Si$ (section 3.3.1) which proved to be essentially amorphous, the films grown on polished $AlN$ at $275-300^0$, yielded highly crystalline films. Some twelve X-ray diffraction peaks, see Table 2, have currently defied unambiguous phase identification. Several of the $h-BN$ peaks are present. The films seem stable in laboratory


Figure 16: Post deposition nucleation of the $H_3BO_3$ reaction product on low-temperature $BN$ films generated on silicon substrates.

air. They did not form any microscopically observable reaction products. Initial X-ray diffractometry showed many distinct diffraction peaks, indicating the presence of crystalline material. Neither $c-BN$ nor hexagonal $BN$ appeared to be the predominant phases. There was reason to believe that the deposit was orthorhombic $BN$, a product of shock wave compression synthesis of hexagene, originally reported by Batsanov et al., in 1965 [53]. Two of its 50% intensity lines were, however, not clearly evident. The possibility of $Si-B-N$ or $Si-O-B-N$ reaction products as well as off-stoichiometry $BN$ alteration products, resulting from impurities in the "binder phase" of the polycrystalline $BN$ target material, also could not be supported. The exact composition of the new phase(s) has not yet been determined.

The diffraction measurements were carried out with a copper anode source ($CuK_\alpha$, $\lambda =$ 1.54 Å). Fig. 17 shows a typical scan. A peak at $2\theta = 26.76$ is consistent with the (002) reflection of $h-BN$ with a lattice constant of 3.328 $\AA$. The value of the lattice constant agrees with the generally accepted value. This also indicates that the film is essentially unstrained. The diffractions from other major peaks of $h-BN$ such as (100) ($2\theta$=41.657, d=2.168Å) and (101) ($2\theta$= 43.8, d=1.83Å) are also present.

The $d$ values of $BN$ films are slightly different from the standard $d$ values in the ASTM files, i.e. d= 2.168 Å for (100) and d= 1.83Åfor (101). This could result from a departure from the stoichiometric $BN$ composition. The inclusion of impurities such as oxygen and an

## TABLE 2

### X-Ray Diffraction Data from Films Generated with *h-BN* Targets onto *AlN* Substrates

| Line number | $2\theta$ (degree) | Intensity* (%) | Identification (preliminary) |
|---|---|---|---|
| 1 | 23.95 | 67 | |
| 2 | 26.76 | 50 | *h-BN* |
| 3 | 30.58 | 8 | |
| 4 | 34.21 | 100 | |
| 5 | 41.73 | 37 | *h-BN* |
| 6 | 42.58 | 33 | |
| 7 | 43.87 | 31 | *h-BN* |
| 8 | 49.05 | 62 | |
| 9 | 50.15 | 35 | *h-BN* |
| 10 | 55.17 | 29 | *h-BN* |
| 11 | 56.16 | 40 | |
| 12 | 61.53 | 35 | |

* Estimated and relative to line No.4 = 100%.

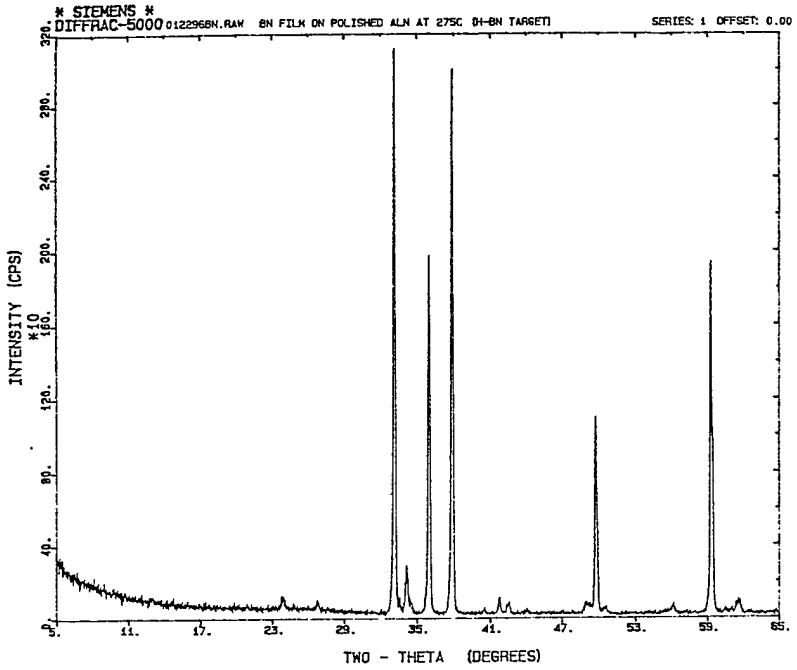


Figure 17: X-ray diffraction pattern of $BN$ thin films deposited on $AlN$ at $275^0$C.

internal stress, might cause the observed peak broadening.

The intensities of the XRD peaks of the $BN$ coatings deposited at $300^0$C were generally weak as compared with those of the polycrystalline $AlN$ substrate, suggesting that the coatings at this deposition temperature were not highly crystalline.

### 3.3.3 $BN$ targets - $Al_2O_3$ substrates

The apparent reactivity of the $AlN$ surface to plasma deposition products from $h-BN$ targets, was not present with $Al_2O_3$ substrates. With both room temperature and elevated temperature substrates ($300^0$C) the films were essentially amorphous, with only some evidence of $H_3BO_3$ as a reaction product with the low temperature substrates. In any case no $h-BN$ or $c-BN$ could be detected. Films prepared with heated substrates also showed no evidence of corrosion. The $Al_2O_3$ substrates therefore yield results very similar to those obtained with $Si$, at least up to $300^0$C.

### 3.3.4 Boron targets - $AlN$ substrates

When polycrystalline boron targets were used, the resultant films were crystalline with both the room temperature and elevated temperature substrates. Several diffraction lines of

hexagonal boron nitride are present. The X-ray diffraction lines for the room temperature films are essentially identical to those obtained with $h-BN$ targets on $AlN$ (see section 3.3.2). The films ($B$ target on $AlN$) at elevated temperatures show several more diffraction peaks. The exact identification still needs further work.

### 3.3.5 $BN$ targets - Nickel substrates

Well-crystallized cubic boron nitride films have been prepared on polycrystalline $Ni$ substrates using a hot filament assisted RF plasma chemical vapor deposition (CVD) method by F. Zhang et al [60]. $Ni$ is one of the few materials that has a close lattice parameter match with $c-BN$ (a = 3.52 Å for $Ni$ and a = 3.612 Å for $c-BN$). Furthermore, $Ni$ is an effective solvent - catalyst metal for diamond crystallization under HPHT conditions. Based on the similarity of $c-BN$ and diamond, it is reasonable to suppose that the $c-BN$ phase may be successfully nucleated on metal $Ni$ substrates while hexagonal $BN$ ($h-BN$) and wurzite $BN$ are effectively suppressed.

We have initiated research on the thin film deposition of $BN$ onto $Ni$ substrates at a substrate temperature of $275^0$C using RF magnetron sputtering and polycrystalline $h-BN$ targets. The substrates were carefully cleaned with acetone and deionized water prior to deposition. Films were deposited in an nitrogen gas environment with 100 W ac power at a frequency of 13.56 MHz.

The use of a metallic substrate, specifically nickel (isostructural with $c-BN$) and an $h-BN$ target, has yielded very smooth films which could be identified as cubic boron nitride. The evidence comes from the persistent occurrence of the 100% peak of $c-BN$ together with the (high intensity) peaks of nickel in the X-ray diffraction pattern of the film - on - substrate samples, see Fig. 18.

There is no indication of crystalline $h-BN$ nor of any other phases. We also could not find any oxidation predicts on the film surfaces even after three months of exposure to humid laboratory air.

Careful (EDX) analysis of the films revealed only boron and nitrogen. Nickel could not be detected, testifying to relatively thick $c-BN$ films. SEM microscopy of the smooth and transparent films revealed a medium grain size of 2 $\mu$m.

**The possibility of generating stable $c-BN$ films by PVD techniques at temperatures as low as $275^0$C, is felt to be a very significant development.**

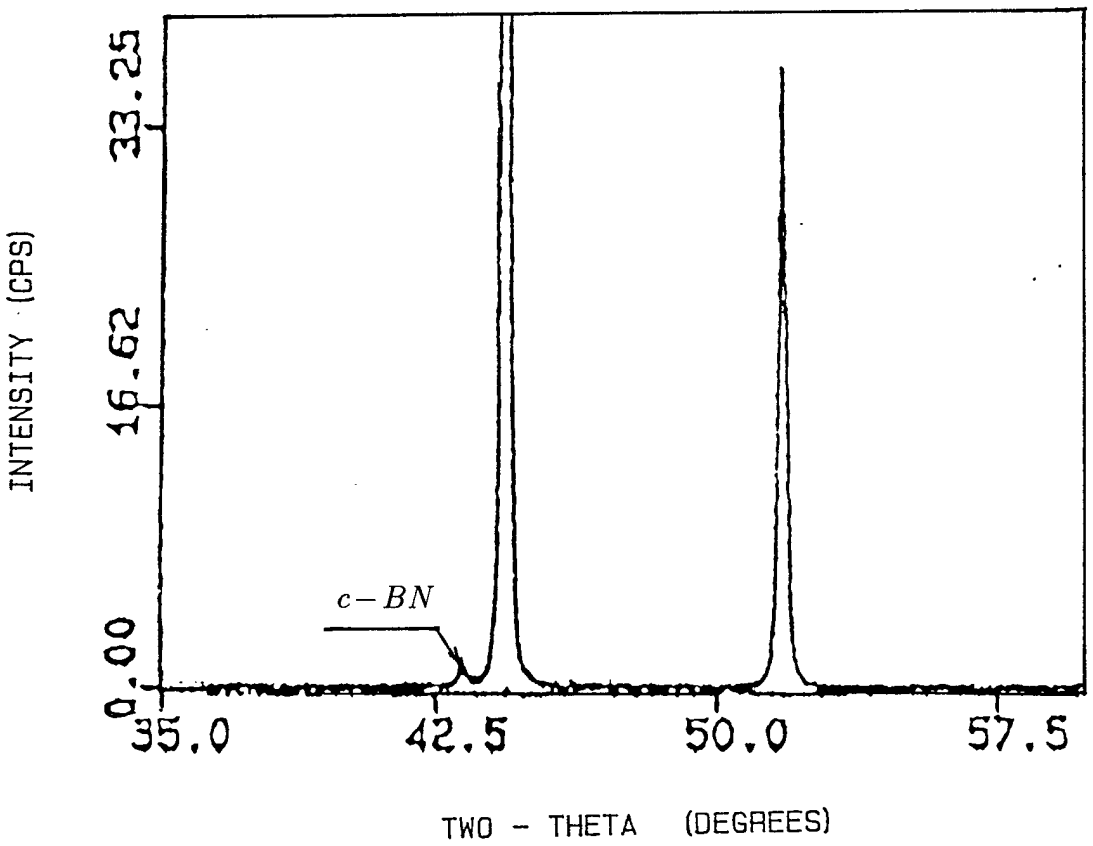


Figure 18: Partial X-ray diffraction pattern
of $c - BN$ thin films deposited on $Ni$ at $275^0$C.

# 4 Deposition of $Si - Al - O - N$ Films

## 4.1 General

The four component $Si - Al - O - N$ system can be represented in tetrahedral form, as in Fig. 19. Each of the vertices can be thought of as representing one atom of the respective elements. A variety of materials, including some widely used high technology oxides and nitrides, such as $Al_2O_3$, $AlN$ and $Si_3N_4$, are members of this system.

Sialon, as a subset of $Si-Al-O-N$, can be produced by reacting appropriate mixtures of $Si_3N_4, AlN, Al_2O_3, SiO_2$, and $Si_2N_2O$ by pseudoisostatic hot pressing in graphite dies. The composition ranges of $\beta\prime$, $X$ and $O$ phase sialons, (Fig. 20), extend in directions in which silicon and nitrogen are increasingly replaced by aluminum and oxygen [61]. Five ordered polytype phases also exist, each with their own solid solution range. They are structurally very similar, based on the wurtzite structure of the parent $AlN$. They are known by their Ramsdell symbols as 15R, 21R, 127R, 12H and 10H [61].

The sialon family of materials represents relatively wide compositional, structural and property variability and provides an excellent opportunity to implement various mechanical and electrical system requirements.

The $\beta\prime$-sialon phase has the same crystal structure as $\beta - Si_3N_4$ with a hexagonal unit cell containing $M_6X_8$. It is generally processed by hot pressing ($1750°C$) and annealing ($1250°C$), a mixture of $\beta - Si_3N_4$, $AlN$, $Al_2O_3$ and $Y_2O_3$, in which the latter acts as an sintering additive [62]. In the pseudo quarternary $Si_3N_4 - AlN - Al_2O_3 - SiO_2$, $\beta\prime - sialon$ extends from the $Si_3N_4$ corner to the $AlN$ composition on the $Al_2O_3 - AlN$ "join" for about 60% of the distance. It has been found that, in reacting $Si_3N_4$ with $Al_2O_3$, $N^{3+}$ in $Si_3N_4$ is replaced by $O^{2-}$ while at the same time $Si^{4+}$ is replaced by $Al^{3+}$, widening the exploration of the reversible replacement [62]

$$Si^{4+}N^{3-} \rightleftharpoons Al^{3+}O^{2-}.$$

Thus $\beta\prime - sialon$ is expressed by $Si_{6-z}Al_zO_zN_{8-z}$ for which $z$ represents the number of $Si^{4+}$ that have been being replaced by $Al^{3+}$. It has a maximum value of 4 [62].

Measurements on compositions containing roughly equal concentrations of silicon and aluminum, $Si_3Al_3O_3N_5$ with $z$=3, show that the physical and mechanical properties are similar to those of $\beta - Si_3N_4$ [62]. Although its thermal conductivity is lower, it has good thermal shock properties. The coefficient of thermal expansion (CTE) ($3.1 \times 10^{-6}/K$) [63] is less than that of $\beta - Si_3N_4$ ($3.5 \times 10^{-6}/K$) [63], and $Si_3Al_3O_3N_5$ has a better compatibility with silicon for which the CTE is $2.6 \times 10^{-6}$/K [64]. Another advantage is that $\beta\prime - sialon$

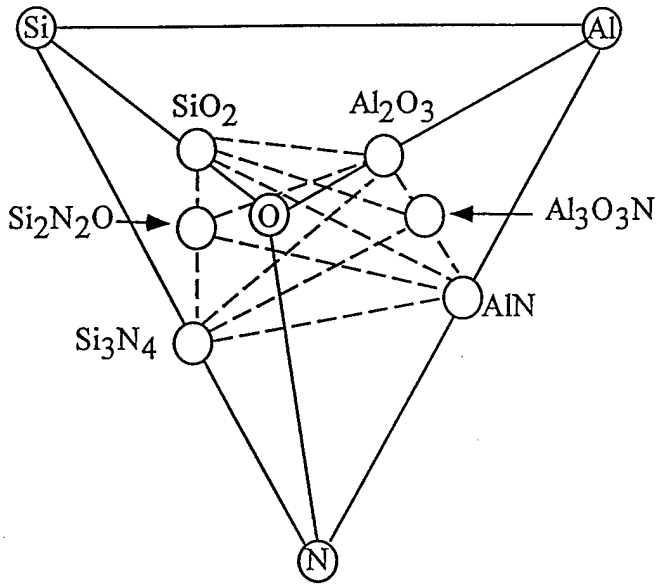


Figure 19: Tetrahedral representation of the $Si - Al - O - N$ system [62].

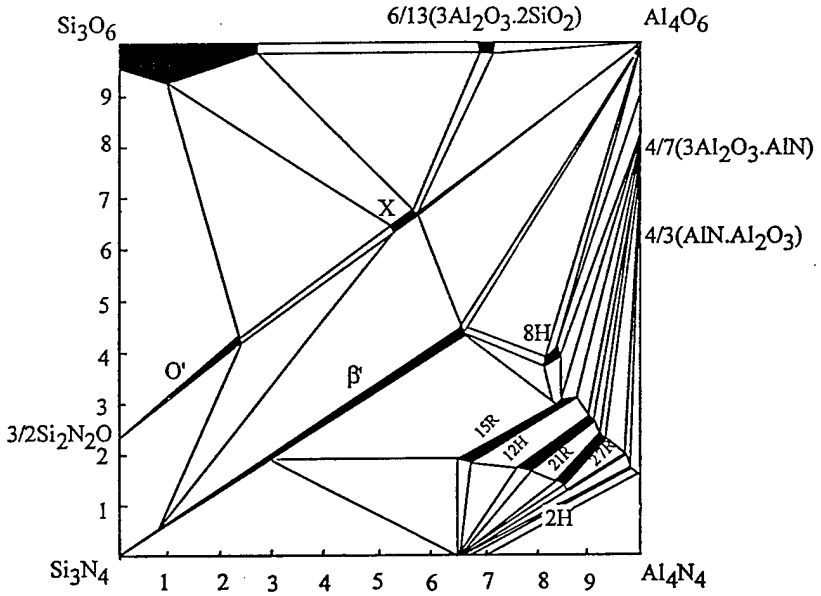


Figure 20: The $Si_3N_4 - AlN - SiO_2$ system [62].

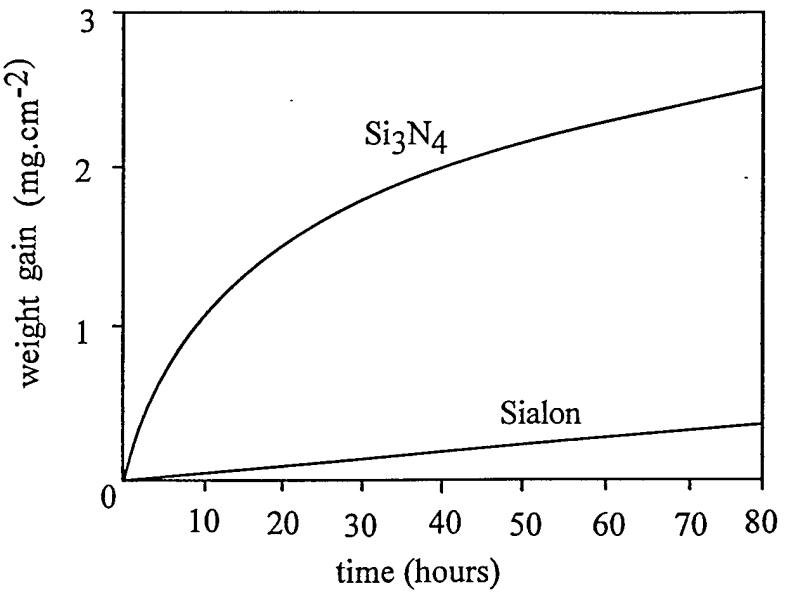


Figure 21: Chemical stability of - sialon compared with - $Si_3N_4$ (oxidation in flowing dry air at $1400^0$C [62].

is much more stable than $\beta - Si_3N_4$, i.e. its oxidation resistance is better than that of silicon nitride [62], see Fig. 21.

Hot-sintered $\beta\prime - sialon$ displays a relative dielectric constant of 8-10 [63], and a dissipation factor of 0.002 [63]. It has been reported that an increase in the $Al^{3+}$ concentration leads to a higher value of the dielectric constant [65]. The introduction of small amounts of titanium to sialon precursor chemistry has yielded bulk type sialon with $\epsilon\prime = 8.5 - 10$, and $tan\delta = 6 \times 10^{-4}$ [65]. Relevant properties of $\beta\prime - sialon$ are compared to some other materials in Table 3.

Research on $\beta\prime - sialon$ has focused on synthesis and mechanical property evaluation. Detailed information can be obtained from the review by K.H. Jack [62]. Dielectric properties have been reported in relatively few papers [65,66], emphasizing only bulk sialons. The thin film deposition of sialon has been reported in one paper only [67]. It deals with the RF magnetron sputtering technique using $\beta\prime - sialon$ targets. The films were described as offering good oxidation and $H_2SO_4$ resistance. The primary objective of the study was the generation of oxidation resistant coatings.

## TABLE 3

**Physical Properties of $Al_2O_3, Si_3N_4$ and $\beta\prime - sialon$**

| Type | Property | $Al_2O_3$ | $Si_3N_4$ | $Sialon$ |
|---|---|---|---|---|
| Electrical and Dielectric Properties | dielectric constant $\epsilon\prime$ | 10 | 6 | $8-10$ |
| | loss factor $tan\delta$ $(\times 10^{-3})$ | 2 | 1 | 2 |
| | breakdown strength $(\times 10^5 V/cm)$ | 9.0 | $1.6-2.0$ | – |
| | resistivity $(\Omega.cm)$ | $10^{14}$ | $10^{14}$ | $10^{12}$ |
| Thermal Properties | thermal conductivity $(W/mK)$ | 35 | 25 | 21.3 |
| | coefficient of thermal expansion $(\times 10^{-6}/K)$ | 8.0 | 3.5 | 3.1 |
| | thermal shock resistance | good | excellent | excellent |
| Mechanical Properties | density $(g/cm^3)$ | 4.0 | 3.2 | 3.2 |
| | tensile strength $(MPa)$ | 206 | 550 | 550 |
| | compressive strength $(MPa)$ | 2500 | 3500 | 3500 |
| | melting point $(^oC)$ | 2055 | 1900 | 1750 |
| Reference | – | [10] | [12] | [12] |

## 4.2 Experimental details and results

In *sialon* film deposition, we have used sintered polycrystalline targets and argon and nitrogen as carrier gasses. The sialon targets, one inch in diameter and 0.119 inch thick, were vendor purchased. Their X-ray diffraction patterns were virtually identical to that of $Si_3N_4$. Some of the diffraction peaks were slightly shifted, indicating an actual composition close to $Si_3N_4$, the end member of the wide compositional range in the $Si-Al-O-N$ quarternary which covers the $\beta$' sialon phase. Sialon films have been deposited on $AlN$ (ground and polished) $MgO$ (ground surfaces only) and silicon (polished, etched and ground ) substrates. All depositions were made on not intentionally heated substrates.

As was reported for the $AlN$ and $BN$ films (section 2 and 3), the surface character of the as-deposited films is primarily determined by the nature of the substrate surfaces. The highly polished substrates produced very smooth $Si-Al-O-N$ films, often "improved" over the underlying surface. The rougher substrate surfaces yield randomly scattering film surfaces which can, relatively speaking, be considered " rough".

The $Si-Al-O-N$ films show a "columnar" growth morphology ("columns" perpendicular to the substrate surface) which leads to very dense films on the lapped substrates. The rougher, ground, surfaces tend to produce lower density films.

Elemental analysis of the target material and the deposited films was carried out with energy dispersive X-ray (EDX) techniques, which could detect silicon, aluminum and nitrogen. Chemical composition of the amorphous films is essentially independent of the type of substrate. Table 4 gives an overview of the results. It will be noted that film composition is not the same as target composition and depends much on the chemical make-up of the plasma growth environment. It was also discovered that the as-deposited films undergo a stabilizing oxidation process when exposed to laboratory air. This is particularly noticeable in films grown in a 100% argon environment. The effect is less when a 100% nitrogen plasma is used. The stabilized films yield enhanced properties for the dielectric constant, loss tangent and breakdown strength of the films, see also [68]. The $Si-Al-O-N$ thin films were deposited by an RF magnetron sputtering system, using a target disk of hot-sintered polycrystalline $\beta\prime$ - sialon with a diameter of 2.54 cm. Silicon (100) wafers were used as substrates. The distance between the targets and substrates was 8 cm. A quartz crystal mounted at the same angle as the substrate and at the same distance from the target source, acted as a film thickness monitor.

The substrates were carefully cleaned with acetone and deionized water prior to deposition. Films were deposited in an argon or nitrogen gas environment with 100 W ac power at a frequency of 13.56 MHz. The substrate temperatures reached about $50^0$C. No external

TABLE 4

**Elemental Distribution in Sialon Target Material and in the Deposited Films**

| SAMPLE | CONCENTRATION (Atomic %) | | | | REMARKS |
|---|---|---|---|---|---|
| | Si | Al | O | N | |
| Sialon target material | 28 | 2 | 10 | 60 | as received |
| Film (initial) | 19 | 1 | 49 | 31 | deposited in 100% argon |
| Film (aged) | 20 | 1 | 64 | 15 | |
| Film (initial) | 22 | 2 | 26 | 50 | deposited in 100% nitrogen |
| Film (aged) | 21 | 2 | 33 | 44 | |

heating was applied to the substrate.

The microstructures of the deposited films were examined by scanning electron microscopy (SEM). Crystallinity and chemical analysis were conducted with X-ray diffractometry and energy-dispersive X-ray spectroscopy (EDS) respectively. An in-house developed Digital Enhanced Scatterometer (DES) and a profilometer were used for surface characterization [1]. Dielectric constants and loss factors were measured with an LCR meter. Electrical resistivity was measured with a set-up designed for I-V characterization consisting of a computer controlled system including a voltage/current source, two multimeters and a 1000 $\Omega$, 10 Watt resistor.

## 4.3 Surface analysis

Three types of silicon (100) wafers were used as substrates [1]. Fig. 22 shows an SEM micrograph of a typical superpolished $Si$ wafer surface. Bumps with vertical dimensions of several nanometer are distributed randomly over the entire surface. Fig. 23 shows a surface of an etched silicon substrate with a roughness of about 2900 $\mathring{A}$. A third substrate type, $R_a$=3450 $\mathring{A}$, was mechanically polished, see Fig. 24. The thin films were deposited on these three different types of silicon substrates under identical conditions, at a pressure about

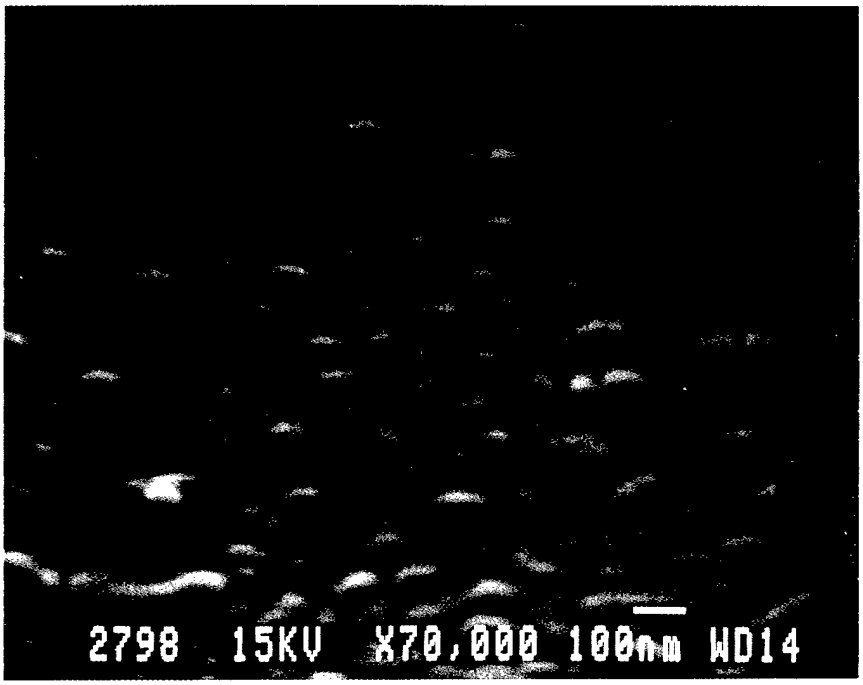


Figure 22: SEM micrograph of a superpolished silicon substrate

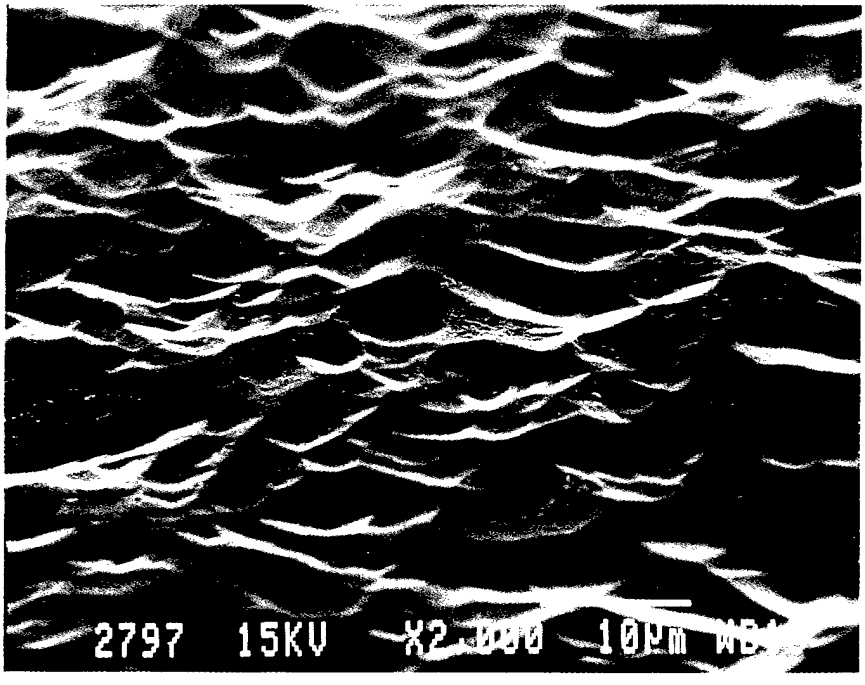


Figure 23: SEM micrograph of an etched silicon substrate surface

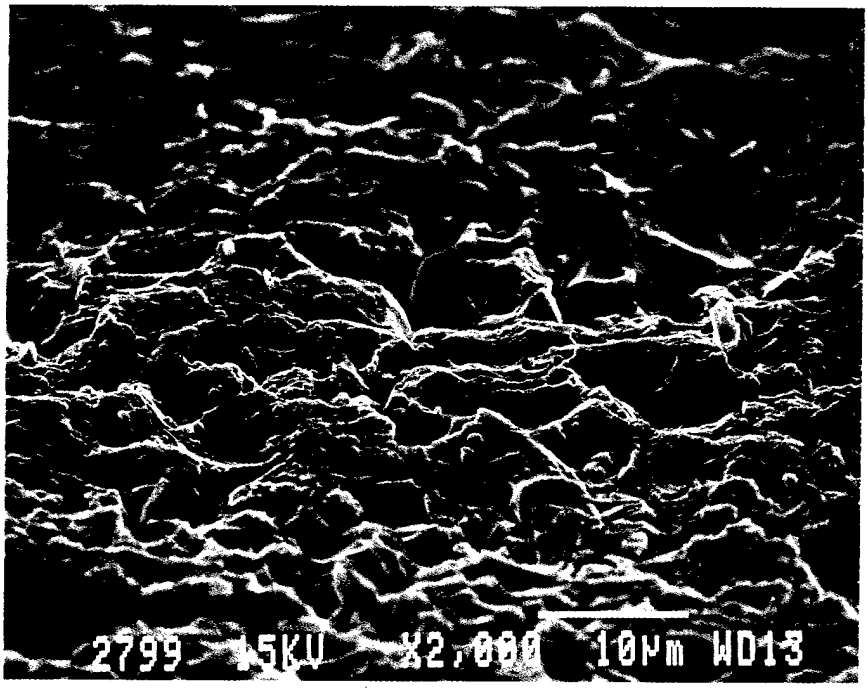


Figure 24: SEM micrograph of a ground silicon substrate surface.

$1.7 \times 10^{-2}$ and 100 W forward power. Fig. 25 is an SEM micrograph of a thin film on a superpolished silicon substrate. The film surface looks very smooth and uniform, although somewhat rougher than the original substrate surface. Small wavelets resulting from the film's columnar growth, can be detected. Fig. 26 shows the top surface and cross-section of a film deposited on an etched silicon surface. The film surface character is comparable to that of the substrate. On the ground silicon substrates, as-deposited films grow as "big tooth" structures, as seen in Fig. 27. The roughness of the as-deposited films on superpolished, etched and ground silicon substrates were 50 Å, 3800 Å, and 3250 Å respectively, see Table 5. As reported for $AlN$ and $BN$ film, on its surface, appears to "mimmick" or "copy" the character of the substrate surface, displaying a roughness that is not much different from that of the substrate itself.

The film structure is affected not only by the substrate roughness but also by the microstructure of the substrate. This conclusion has been supported by our optical scattering measurements. The power spectral density (PSD) of the as-deposited film surfaces relative to the spatial frequency are shown in Fig. 28.

The PSD curve of the $Si-Al-O-N$ film is virtually identical to that for the superpolished silicon substrate surface. Whether film surfaces are rougher than that of the substrate surface can be deduced easily by integration of the area under each of the PSD curves, which

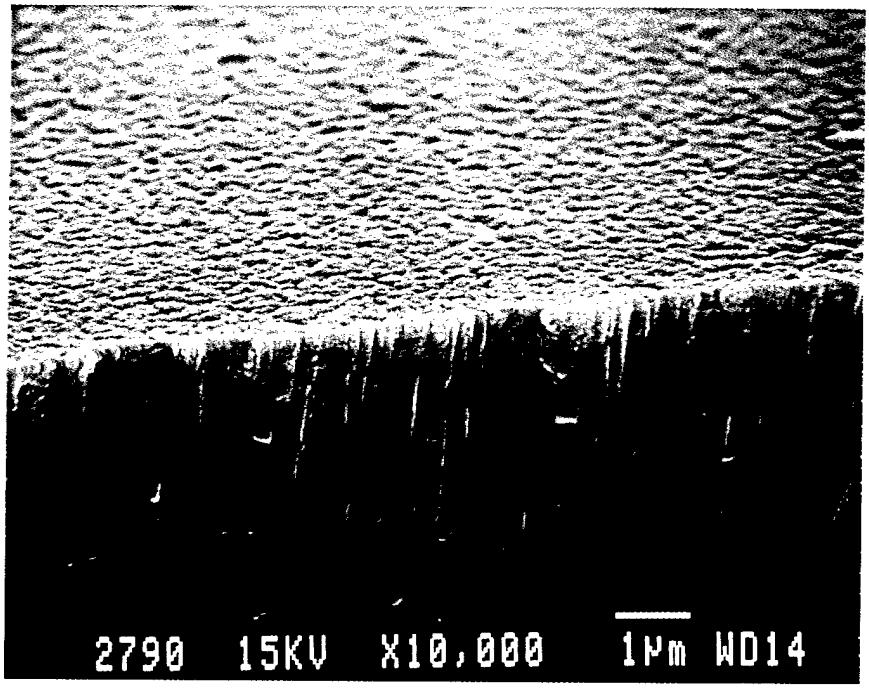


Fiqure 25: SEM micrograph of a $Si - Al - O - N$ film on a superpolished silicon substrate (substrate not visible).

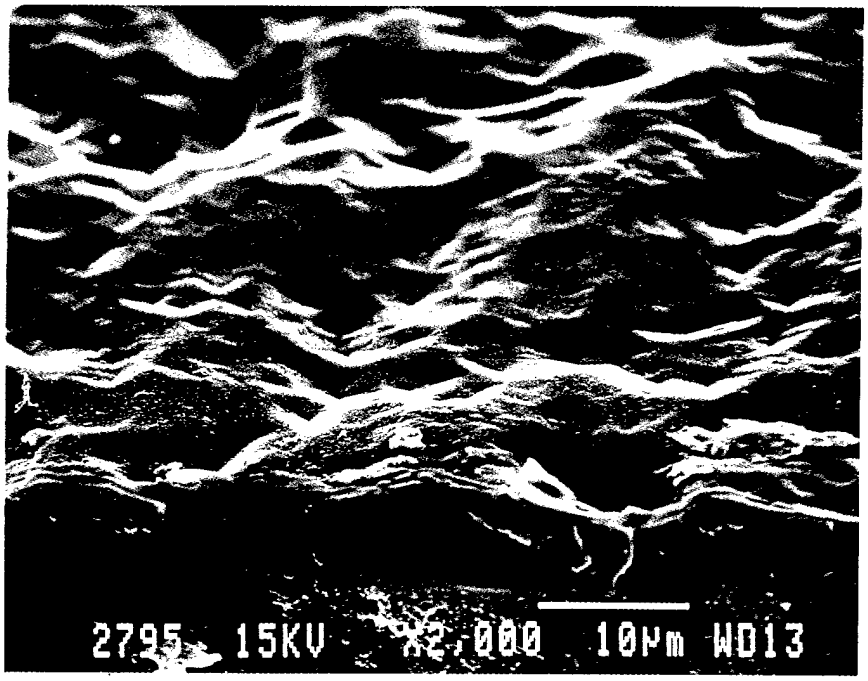


Figure 26: SEM micrograph of a $Si - Al - O - N$ film on an etched silicon substrate.

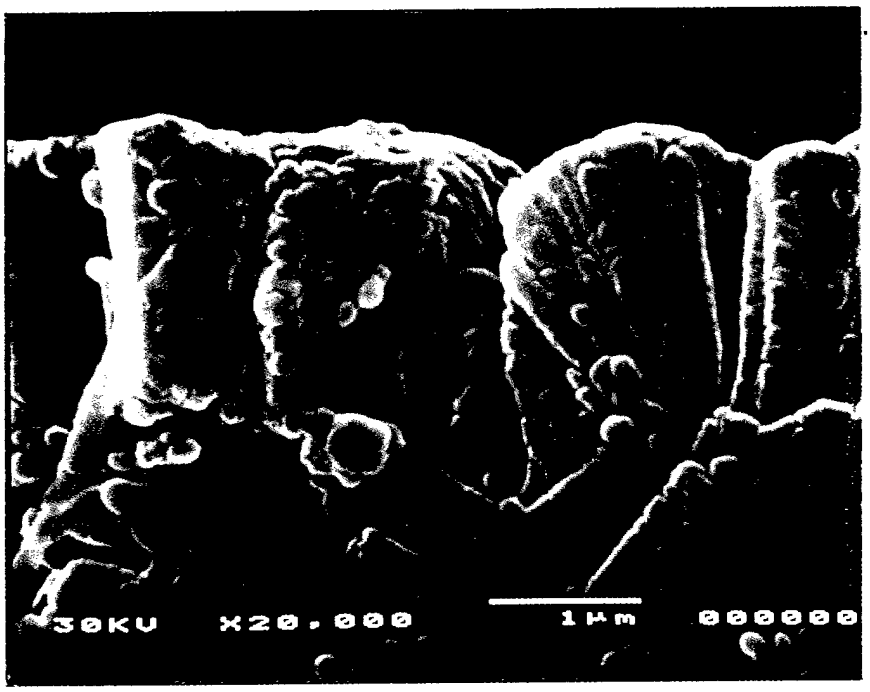


Figure 27: SEM micrograph of a $Si-Al-O-N$ film on a ground silicon substrate.

Table 5

Surface Roughness of Substrates and Films Deposited on those Substrates

| Sample Type | Arithmetic Average Roughness Ra(Å) | Total Indicated Runout TIR(Å) |
|---|---|---|
| Si substrate superpolished | 50 | 350 |
| $Si-Al-O-N$ film | 50 | 500 |
| Si substrate etched | 2,900 | 21,300 |
| $Si-Al-O-N$ film | 3,800 | 20,750 |
| Si substrate ground | 3,450 | 21,500 |
| $Si-Al-O-N$ film | 3,250 | 19,500 |

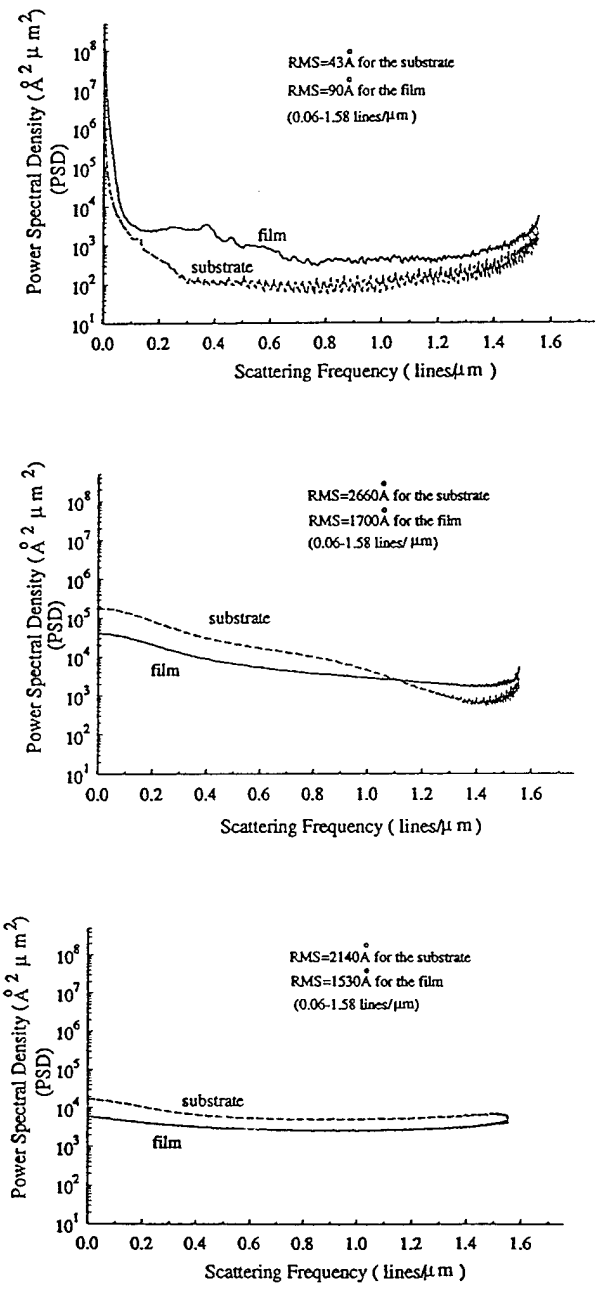


Figure 28: PSD vs. scattering frequency for a $Si - Al - O - N$ film on polished (top), etched and ground (bottom) silicon substrates.

yields the RMS roughness value. On ground silicon surfaces, the film and the substrate reveal similar surface character throughout the entire frequency range, while the films deposited on etched silicon, indicate a considerable difference in character as compared to that of their substrates. The original etched substrate surfaces show higher reflectance near the specular direction, and less (light)scattering out of the reflection direction compared to that of their films. The as-deposited films on ground substrates and the substrates themselves are typical of randomly scattering surfaces and can be considered "rough".

Differences in film thickness were detected on the three types of silicon substrates, in spite of identical deposition conditions. The films on the superpolished substrates had a thickness of about 4 $\mu$m while the films on the etched and ground surfaces were 5.5 $\mu$m and 6 $\mu$m thick respectively. Reasons for this may be that the films formed on the superpolished substrates were of higher density, or that the sputtered particles are more easily re-evaporated (dislodged) after initial adsorption due to surface smoothness [69].

## 4.4 Dielectric characterization

Capacitor structures were formed by depositing $Si - Al - O - N$ films in 100% $Ar$ gas onto $Al$ base-electrodes. X-ray diffraction analysis of as-deposited films revealed a uniform and homogeneous amorphous structure. The thicknesses of the dielectric layers ranged form 1-2$\mu$m, depending on deposition time. Five samples were tested for each film type. The resistivities of the films deposited in 100% $Ar$ ranged from $4.14 \times 10^8$ $\Omega$cm to $6.18 \times 10^9$ $\Omega$cm. The average for all samples was $4.78 \times 10^9$ $\Omega$cm. The dielectric constants of as-deposited films ranged from 3.4 to 2.9, and the loss factor increased from 0.003 to 0.012 as the frequency increased from 10 kHz to 1 MHz, as shown in Fig.27.

Thin films deposited in 100%$N_2$ revealed a higher nitrogen content. The resistivities of these films ranged from $7.00 \times 10^9$ $\Omega$cm to $3.42 \times 10^{10}$ $\Omega$cm. The average for all samples was $1.91 \times 10^{10}$ $\Omega$cm. The dielectric properties of these films showed a trend similar to those deposited in 100% $Ar$. The dielectric constants decreased from 4.7 to 3.9 and loss factors increased form 0.0006 to 0.012 as the frequency increased form 10kHz to 1MHz, see Fig. 29. A comparison of the values for resistivity, dielectric constant, loss factor and elemental concentration of the as-deposited films is shown in Table 6. The increase in dielectric constant with decrease of frequency may be attributed to interfacial polarization in this frequency region. The reduction of the dielectric constant of the films, compared to that of the original $\beta\prime$-sialon target, can be explained by an increase in oxygen vacancies and the amorphous structure of the films. The sharp rise in the loss factor from 100kHz to 1MHz is due to the polarization of the bipoles in the deposited materials which, apparently,

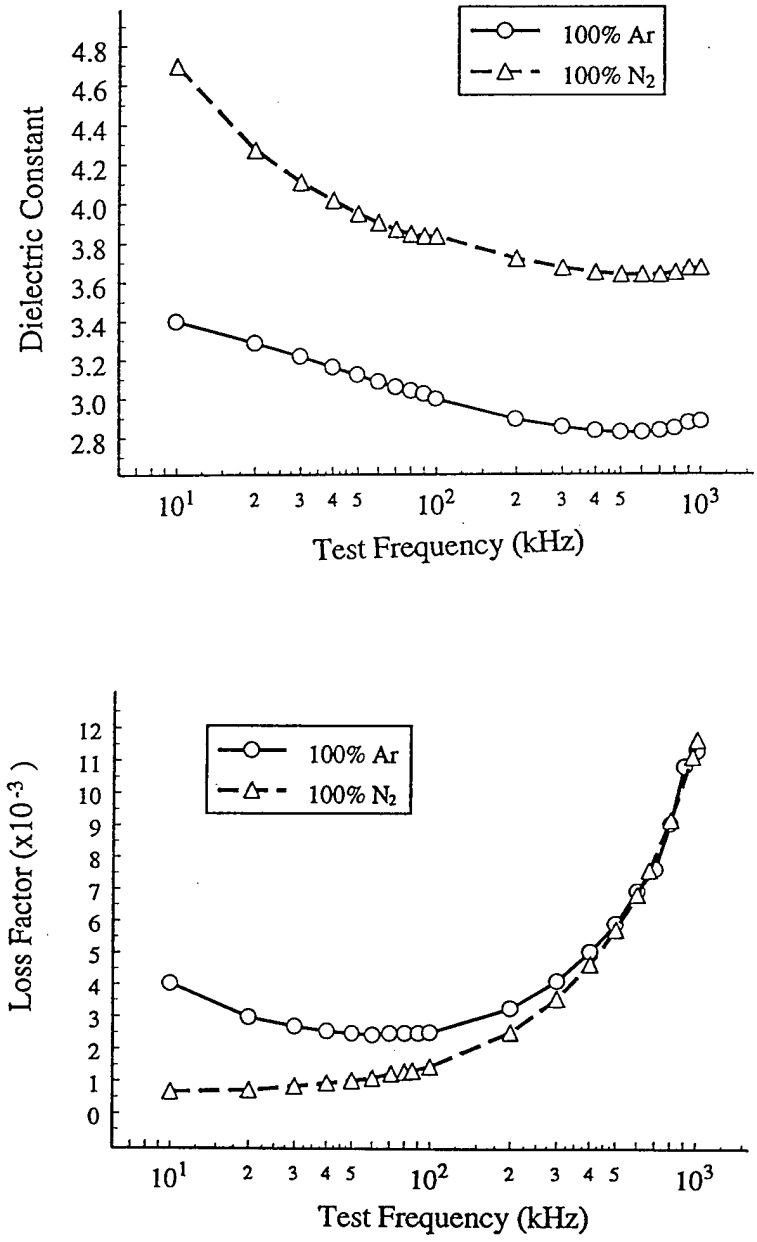


Figure 29: Dielectric constant and loss factor vs. frequency of as-deposited amorphous $Si - Al - O - N$ films, grown in different environments.

Table 6

Comparison of Dielectric Properties
of As-Deposited $Si - Al - O - N$ Films

| Material Type | Resistivity ($\Omega cm$) | Dielectric Constant (1MHz) | Loss Factor (1MHz) |
|---|---|---|---|
| Si-Al-O-N Films in 100%$Ar$ | $4.78 \times 10^9$ | 2.90 | 0.011 |
| Si-Al-O-N Films in 100%$N_2$ | $1.91 \times 10^{10}$ | 3.70 | 0.012 |
| $\beta\prime - sialon$ Solid Targets | $2.50 \times 10^{11}$ | 10.01 | 0.0001 |

cannot follow the changes at these higher frequencies.

The as-deposited films with higher nitrogen concentrations exhibited higher dielectric constants, lower loss factors and higher electrical resistivity values. An increase in $Al$ ion content in the films lead to similar results, as was also found to be the case with bulk polycrystalline $\beta\prime$-sialon [72].

# 5 Summary and Conclusions

The primary goal under the contract, that of providing a vapor deposition facility for the deposition of thin films for structural and electronic applications, preferably at low cost, has been reached.

It has been possible to extend our work into the generation and evaluation of films in the systems $AlN$, $(Al,B)N$, $c-BN$ and *Sialon.* We have shown that such films and film structures (devices) can potentially be used as: high thermal conductivity substrates and in device coating applications ($AlN$); for high and low power capacitor storage devices (*sialon*); in systems with broad "property engineering capabilities" *(Al, B)N*; as wide bandgap materials for e.g. high efficiency electron emission surfaces (cold cathodes); as high wear resistant and high-strength materials; when doped, as discrete and integrated passive and active devices.

Specific results for the three materials systems are briefly summarized below:

- Thin films of $AlN$, $(Al,B)N$ and $Si-Al-O-N$, both amorphous and crystalline, have been successfully deposited by physical vapor deposition (PVD) techniques.
- Dense and transparent amorphous films of $AlN$ could be deposited from $AlN$ targets onto room temperature substrates.
- Transparent crystalline films of $AlN$ were generated at substrate temperatures as low as $250^0$C.
- The use of $BN$ targets resulted in only amorphous $(Al,B)N$ films, under all conditions, and on all substrates other than on $AlN$.
- PVD from $BN$ or boron targets onto heated ($250^0$C up) $AlN$ substrates yields crystalline films of a complex chemistry and structure which, in both cases, have not yet been determined .
- The amorphous $(Al,B)N$ films deposited onto room temperature substrates readily reacted with laboratory air to form a dense layer of morphologically very well developed $H_3BO_3$ crystallites.

- The surface character of the as-deposited films tends to conform to that of the substrate. Films deposited onto highly polished surfaces often have RMS roughness and surface wavelength values that rival those of the underlying substrates.
- PVD deposition using boron targets onto nickel substrates heated to $275^0$C or above have yielded polycrystalline *c-BN* films. Possible surface reaction products have not been observed, even after several months of exposure to laboratory air.

# References


1. M. Tu, Y. Xu, I. Kulisic, and P. J. Gielisse, "Application of optical scattering in multi-chip module processing," *Proceedings SPIE's International Symposium on Optical Science, Engineering and Instrumentation,* **2541-09** (1995).

2. ASTM X-ray diffraction file number 25-1133.

3. H. M. Liaw, W. Cronin and F. S. Hickernall, *Proc. IEEE Ultrasonics Symp.*, Baltimore, MD., p267, (1993).

4. N. Tirole, A. Choujaa. D. Hauden, G. Martin, P. Blind, M. Froelicher, J .C. Pommier and A. Cachard, *Proc. IEEE Ultrasonics Symp.*, Baltimore, MD. p371, (1993).

5. M. A. Odintzon, N. I. Sushentzov and T. L. Kudryavtzev, *Sens.Act.,* **A 28**, p203, (1991).

6. Y. Lee Woo, W. J. Lackey and P.K. Agrawal, *J. Am. Ceram. Soc.* **74**, p1821 (1991).

7. J. Bauer, L. Biste and D. Bolze, *Phys. Stat. Sol.,* **A 39**, p173 (1977).

8. N. Kuramoto, H. Taniguchi and I. Aso, *Ceram. Bull.,* **68**, p883 (1989).

9. W. M. Yim, E. J. Stofko, P. J. Zanzucchi, J. I. Pankove, M. Ettchberg, and S. L. Gilbert, *J. Appl. Phys.,* **44**, p292 (1973).

10. J. L. Dupuie and E. Gulary, *Appl. Phys. Lett.,* **59**, p549 (1991).

11. M. Morita, S. Isogai, N. Shimizu, K. Tsubouchi and N. Mikoshiba, *Jap. J. Appl. Phys.,* **20**, L173 (1981).

12. L. M. Sheppard, *Ceram. Bull.,* **69**, 1801 (1990).

13. K. Tsubouchi, K. Sugai and N. Mikoshiba, *Jap.J.Appl.Phys.,* **19**, L751 (1980).

14. W. Y. Lee, W. J. Lackey and P. K. Agrawal, *J.Amer.Ceram.Soc.,* **74**, p1821 (1991).

15. J. H. Edgar, Z. J. Yu and B. S. Sywe, *Thin Solid Films,* **204**, p115 (1991).

16. S. Yoshida, S. Misawa, Y. Fujii, S. Takada, H. Hatakawa, S. Gonda and A. Itoh, *J. Vac.Sci. Technol.,* **16** p990 (1979).

17. A. J. Shuskus, T. M. Reeder and E. L. Paradis, *Appl. Phys. Lett.,* **24**, p155 (1974).

18. F. Takeda, T. Mori and T. Takahashi,*Jap.J.Appl.Phys.,* **20**, L169 (1981)

19. K. Tominga, S. Iwamura, Y. Shintani and O. Tada, *ibid,* **22**, p418 (1983)

20. G. L. Huffman, D. E. Fahnline, R. Messier and L. J. Pilione, *J. Vac.Sci. Technol.,* **A 7**, p2252 (1989).

21. M. Mieno and T. Yoshida, *Jap.J.Appl.Phys.,* **29**, L1175 (1990).

22. K. Bewilogua, J. Buth, H. Hubsch and M. Grischke, *Diamond and Related Materials* **2** p1206 (1993).

23. K. Bewilogua, A. Schuetze, S. Kouptsidis and H. Luethje, in "Applications of Diamond Films and Related Materials": Third International Conference, Gaithersburg, MD, Editors: A. Feldman, Y. Tzeng, W. A. Yarborough, M. Yoshikawa, and M. Murakawa, p831 (1995).

24. Hwan-Chul Lee, Jai-Young Lee, *J. Mater. Sci: Materials in Electronics,* **5**, p221 (1994).

25. M. Penza, M. F. De Riccardis, L. Mirenghi, M. A. Tagliente, E. Verona, *Thin Solid Films,* **259**, p154 (1995)

26. M. Akiyama, H. Rezakokabi, K. Nonaka, K. Shobu, and T. Watanabe, *J. Am. Ceram. Soc.*, **78**, [12] p3304 (1995).

27. M. Morita, N. Uesugi, N. Shimizu, K. Tsubouchi and N. Mikoshiba, *Jap. J. Appl. Phys.*, **20**, 17 (1981).

28. A. J. Noreika and D. W. Ing. *Jap. J. Appl. Phys.*, **39**, p5578 (1968).

29. H. Komiyama and T. Osawa, *Jap. J. Appl. Phys.*, **24**, L795 (1985).

30. Y. S. Toulouvian, R. K. Kiby, R. E. Tylor and T. Y. R. Lee, *Thermal Properties of Materials*, **13**, 154 IFI/Plenum, NY-WA., (1977).

31. H. Saitoh, Y. Hirotsu and Y. Ichinose, *J. Jpn. Inst. Metals,* **54**, p562, (1990).

32. T. Goto, T. Tanaka, H. Masumoto, T. Hirai, *J. Mater. Sci., Materials in Electronics* **5**, p324 (1994).

33. C. Weissmantel, K. Bewilogua, K. Brever, D. Dietrich, V. Eversbach, H. T. Erler, B. Rau and G. Reisse, *Thin Solid Films,* **96**, p562 (1990).

34. D. J. Kester and R. Messier, *J. Appl. Phys.,* **72 (2)**, p504 (1992).

35. M. Mieno and T. Yoshida, *Jpn. J. Appl. Sci.,* **29**, L1175 (1990).

36. K. Bewilogua, J. Buth, H. Hubsch and M. Grischke, *Diamond Relat. Mater.,* **2**, p1206 (1993).

37. K. Tominaga, H. Imai and M. Shirai, *Japan. J. Appl. Phys.*, **30**, p2574 (1991).

38. M. Akiyama, H. Rezakokabi, K. Nonaka, K. Shobu, and T. Watanabe, *J. Am. Ceram. Soc.*, **78**, [12] p3304 (1995).

39. M. Sokolowski, J. Cryst. Growth, **46**, p136 (1979).

40. C. Weissmantel, K. Bewilogwa. K. Bruer, D. Dietrich, U. Ebersbach, H-J. Erler, B. Rau and G. Reisse, *Thin Solid Films*, **96**, p31 (1982).

41. S. Shanfield and R. Wolfson, *J. Sci. Technol.,* **A 1**, p323 (1983).

42. K.L. Chopra, V. Agrawal, V.D. Vankar, C.V. Deshpandey and R.F. Bunshah, *Thin Solid Films*, **126**, p307 (1985).

43. K. Inagava, K. Watanabe, H. Ohsone, K. Saitoh and A. Itoh, *J. Vac. Sci. Technol.,* **A 5**, p2696 (1987).

44. H.D. Wiggins, C.R. Aita and F.S. Hickernell, *J. Vac. Sci. Technol.,* **A2**, p322 (1984).

45. P.S. Arya and A. D'Amico, *Thin Solid Films*, **157**, p267 (1988).

46. D.R. McKenzie, D.J.H. Cockayne, D.A. Muler, M. Murakawa, S. Miyake and S. Watanabe, *J. Appl. Phys.,* **70**, p3007 (1991).

47. Proposal "Materials development for high performance MCM's and devices" submitted to U.S. ARMY, ARL Dec.1993.

48. A. Bath, P.J. van der Put, J.G.M. Becht, J. Schoonman and B. Lepley, *J. Appl. Phys.,* **70**, p4366 (1991).

49. S. Komatsu, Y. Moriyoshi, M. Kasamatsu and K. Yamada, *J. Appl. Phys.,* **70**, p7078 (1991).

50. S. Komatsu, Y. Moriyoshi, M. Kasamatsu and K. Yamada, *J. Phys. D: Appl. Phys.,* **24**, p1687 (1991).

51. G.L. Doll, J.A. Sell, C.A. Taylor II and R. Clarke, *Phys. Rev.,* **B 43**, p6816 (1991).

52. A. Sokolowska and A. Olszyna, *J. Cryst. Growth,* p507 (1992).

53. S.S. Batsanov, G.E. Blokhina and A.A. Deribas, *J. Struct. Chem.,* (USSR), **6**, p209 (1965).

54. R.H. Wentorf Jr., *J. Chem. Phys.,* **36**, p1990 (1961).

55. L.Vel, G. Demazeau and J. Etourneau, *Mater. Sci. Eng.*, **B10**, p149 (1991).

56. P.J. Gielisse and M. Doser, "Thermistor device and method of producing said device", U.S. Patents No.3,435,399 and No.3,435,398.

57. O. Mishima, J. Tanaka, S.Yamaoka and O. Fukunaga, *Science*, **238**, p181 (1987).

58. O. Mishima, K. Era, J. Tanaka and S. Yamaoka, *Appl. Phys. Lett.*, **53**, p962 (1988).

59. M. J. Rand and J. F. Roberts, *J. Electrochem. Soc.: Solid State Science,* **115(4)**, p423 (1968).

60. F. Zhang, Y. Guo, Z. Song, and G. Chen, *Appl. Phys. Lett.,* **65**(8), p971(1994).

61. P. J. Gielisse, " Materials Development for High Performance MCM's and Devices," *Processing Thin Film Capacitor Structures for High Performance Storage Applications,* DAAL01-94-K-3424, (1994).

62. K. H. Jack, "Review: Sialons and Related Nitrogen Ceramics," *J. Mater. Sci.,* **11**, p1135 (1976).

63. R. Kamo and W. Bryzik, *Ceram. Eng. Sci. Proc.,* **5**, [5-6] p312 (1984).

64. G. K. White, *Experimental Techniques in Low-Temperature Physics.* Clarendon Press, Oxford, 1979.

65. V. Petrovski, *Key Engineering Materials,* **89-91**, p455 (1994).

66. D. S. Perera, D. P. Thompson and J. S. Thorp, *Brit. Cer. J.,* **2**, p57 (1989).

67. O. Knotek, F. Loffler and W. Beele, *Key Engineering Materials,* **89-91**, p275 (1994).

68. Yang Xu, "$Si-Al-O-N$ thin films for capacitor applications", M.S. Thesis, FAMU-FSU College of Engineering, The Florida State University (1996).

69. L. Eckertova, Physics of thin films, second editor, Plenum Press, New York and London, (1986).

# 6 Appendix

**VAPOR DEPOSITION EQUIPMENT AND THIN FILM PROCESSING**

FINAL PROGRESS REPORT

August 1996
DAAH04-93-G-0492

## 6.1 Statement of the problem studied

Provision of vapor deposition equipment towards the realization of thin films and multiple thin film structures of various types and chemistries, for a variety of electronic and structual materials applications.

Specific systems for which films and structures have been realized and evaluated here included: $AlN$; $(Al,B)N$; $BN$; $c-BN$; and Sialon.

## 6.2 Summary of the most important results

See also the Conclusion section of this report, starting on page 41.

1. First time realization of sialon films and structures (devices) for capacitor storage and other electronic applications.
2. Synthesis of crystalline $AlN$ and $(Al,B)N$ thin films at low (250 $^0$C) substrate temperatures for electronic substrate and multichip module coatings
3. The development of a process for the growth of cubic $BN$ ($c-BN$) films at low (250$^0$C) substrate temperatures which are fully stable at ambient laboratory conditions.
4. An M.S thesis "$Si-Al-O-N$ Thin Films for Capacitor Applications" finalized under ARO sponsorship.

## 6.3 List of all publications and technical reports generated under (partial) ARO sponsorship

1. Y. Xu, P.J. Gielisse, N. Bai and M. Tu, "$Si-Al-O-N$ Thin Film Deposition for Integrated Circuitry," Florida ISHM 1996 Technical Symposium, March 21, Orlando, Florida.
2. P. J. Gielisse, "Mechanical Properties of Diamond - Diamond Films and Related Materials," Handbook of Diamond Properties, Eds. M.J.Prelas, K. Bigelow and G. Popovici, Marcel Dekker N.Y.; N.Y. (1996).

3. P. J. Gielisse and D. Yang, "Choice of Substrate Materials in Thin Film Deposition of Wide-Bandgap Superhard Materials," *Third International Conference on Applications of Diamond Films and Related Materials,* National Institute of Standards and Technology special publication 885, Washington, DC, Aug., 1995.

4. P. J. Gielisse, M. Tu, Y. Xu, D. Yuan, and I. Kulisic, "The Role of Surface Characterization in Multi Layer Electronic Structures," North Florida Chapter of ISHM 1995 Technical Symposium, March 21, Orlando, Florida. Proceedings ISHM'95 **A3** (1995).

5. P.J. Gielisse, "The Role of the Substrate in Processing MCM's," invited paper at International Seminar on Multichip Modules, Institute of Electronic Technology Technical University of Wroclaw, Poland, May 11, (1995).

6. P.J. Gielisse, "Synthesis and Applications of III-V Nitrides - Future Challenges," invited paper at C-BN & D'95 *International Conference on C-BN and Diamond Crystallization under Reduced Pressure,* Jablonna, Poland, June 27-29, (1995).

7. P.J. Gielisse, Y. Xu, N. Bai, and H. Niculescu, "Thin Film Deposition for High Energy Storage Applications," C-BN & D'95 *International Conference on C-BN and Diamond Crystallization under Reduced Pressure,* Jablonna, Poland, June 27-29, (1995).

8. M. Tu, Y. Xu, I. Kulisic, and P. J. Gielisse, "Application of Optical Scattering in Multi-Chip Module Processing," *SPIE's International Symposium on Optical Science, Engineering and Instrumentation,* **2541-09**, July, (1995).

9. D. Yuan, M. Tu, H. Niculescu, and P.J. Gielisse, "Choice of substrate materials in thin film deposition of wide-bandgap superhard materials," *3rd International Conference on the Applications of Diamond Films and RElated Materials,* Gaithersburg, Maryland 20899-0001, U.S.A., Aug. 21-24, 1995.

10. P.J. Gielisse, H. Niculescu, D. Yuan, R. Schmidmeier, and K. Chen, "Modeling Stress Distributions in Multi-Chip Module (MCM) Structures," *International Conference on Electronic Technologies,* Windsor, England, June 6-8, (1994). Proceedings ICET'94 p.227-232.

11. P. J. Gielisse, "Advances in Ceramic Multi-Chip Modules (MCM) and High Performance Electronic Materials," NATO Advanced Research Workshop (NATO ARW), Islamorada, FL, June, (1994).

12. P. J. Gielisse and H. Niculescu, "Macro- and Micro-structural Factors Affecting Thin Film Growth of III-V Compounds," *NATO Advanced Workshop on Wide Bandgap Electronic Materials,* Minsk, Belarus, May 4-6, (1994), to be published in NATO ARW Proceedings, Kluwer Academic Publishers, Dordrecht, Netherlands.

13. P. J. Gielisse, M. Tu, D. Yuan, and I. Kulisic, " Surface Characterization in Multi Chip Module Processing," ISHM'94 Technical Symposium, Orlando, FL, March 1994, *ISHM'94 Proceedings*, August (1994).

## 6.4 list of all participating scientific personnel

| | | |
|---|---|---|
| Peter J. Gielisse, | Ph.D | Proffesor Mechanical Engineering,<br>Director, Materials Processing and Application Laboratory |
| Halina Niculescu, | Ph.D | Research Scientist |
| Meirong Tu, | Ph.D | Research Scientist |
| Nai-Zhi Bai | M.S. | Research Scientist |
| Yang Xu | M.S. | Research Assistant,<br>M.S. conferred under ARO sponsorship<br>Thesis: "Si-Al-O-N Thin Films for Capacitor Applications" |

## 6.5 Report of inventions

"Low Temperature Physical Vapor Deposition Process for the Generation of Crystalline $c - BN$ Thin Films and Structures Thereof."

Disclosure letter submitted internally, December 1996.